HASP 2013

Science Report on Payload # 7 of

University of North Dakota and University of North Florida

Development of free flying payload to measure ozone profile in the stratosphere using improved nanocrystalline sensor arrays and radio payload on a high altitude balloon platform

Students Team Leaders:

Marissa Saad (Leader) and Jonathan Wade Snarr (Consultant) (UND)

Students Team: Kenneth Emanuel (UNF)

Faculty Advisors:

Dr. Nirmalkumar G. Patel

Department of Physics, University of North Florida (UNF), Jacksonville, FL 32224

and

Dr. Ron Fevig

Department of Space Studies, University of North Dakota (UND), Grand Forks, ND 58202

Introduction and Aim

After success of the HASP flights made during 2008 to 2012, University of North Dakota (UND) and University of North Florida (UNF) team decided to go for the HASP2013 balloon flight to measure the ozone profile in the stratosphere again using a improved version of payload consist of the nanocomposite ozone sensors, the pressure sensor, GPS and improved version of software and microcontroller circuit. About 90% of ozone is concentrated between 15 and 30 kilometers above the earth's surface (stratospheric ozone). It is also found at ground level in lower concentrations where it is a key component of smog over major cities (tropospheric ozone). The atmospheric layers defined by changes in temperature are shown in fig.1 (a), while the presence of ozone layer in the stratosphere is shown in fig. 1(b).

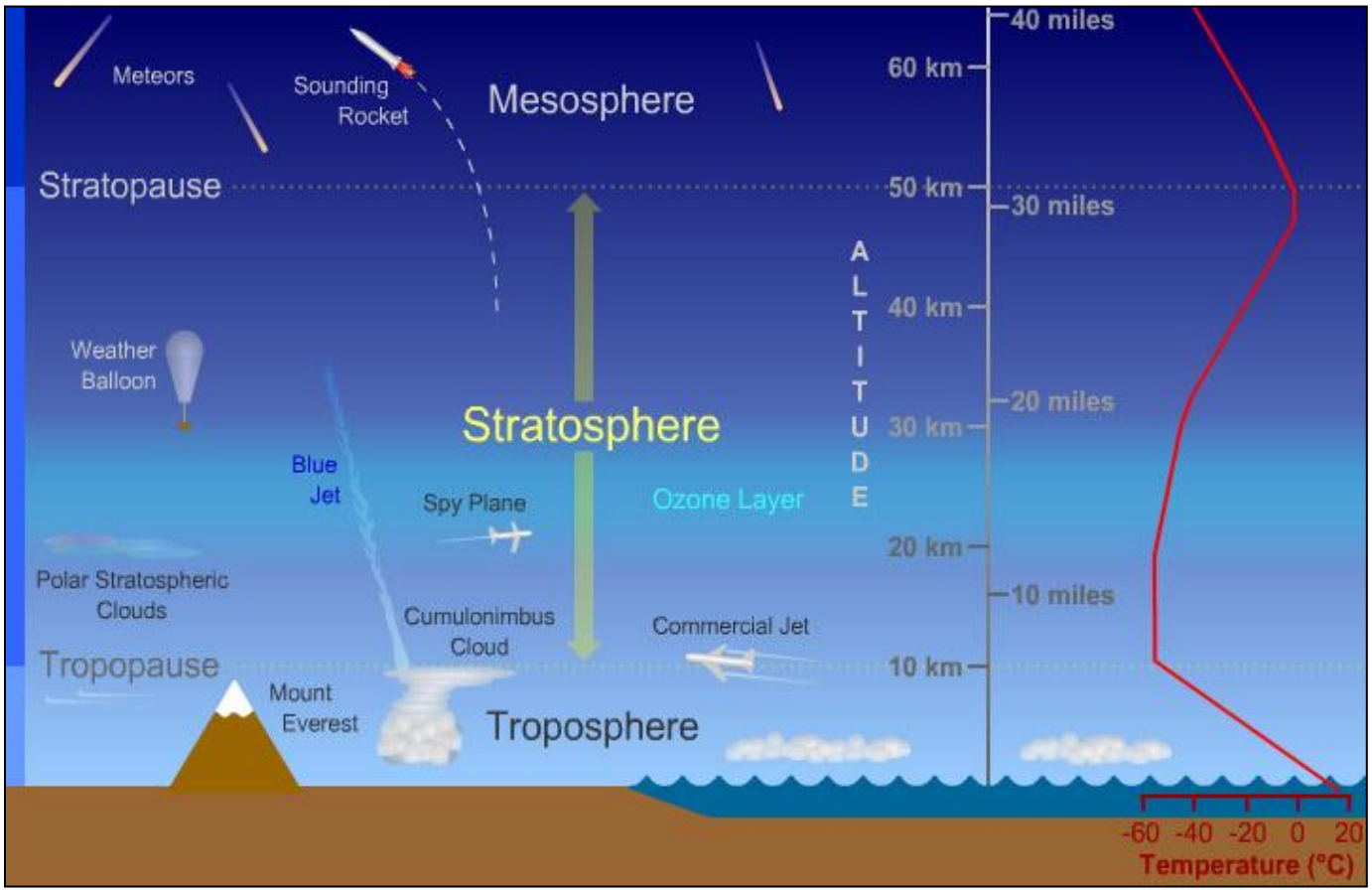

Fig.1 (a) shows the atmospheric layers defined by changes in temperature

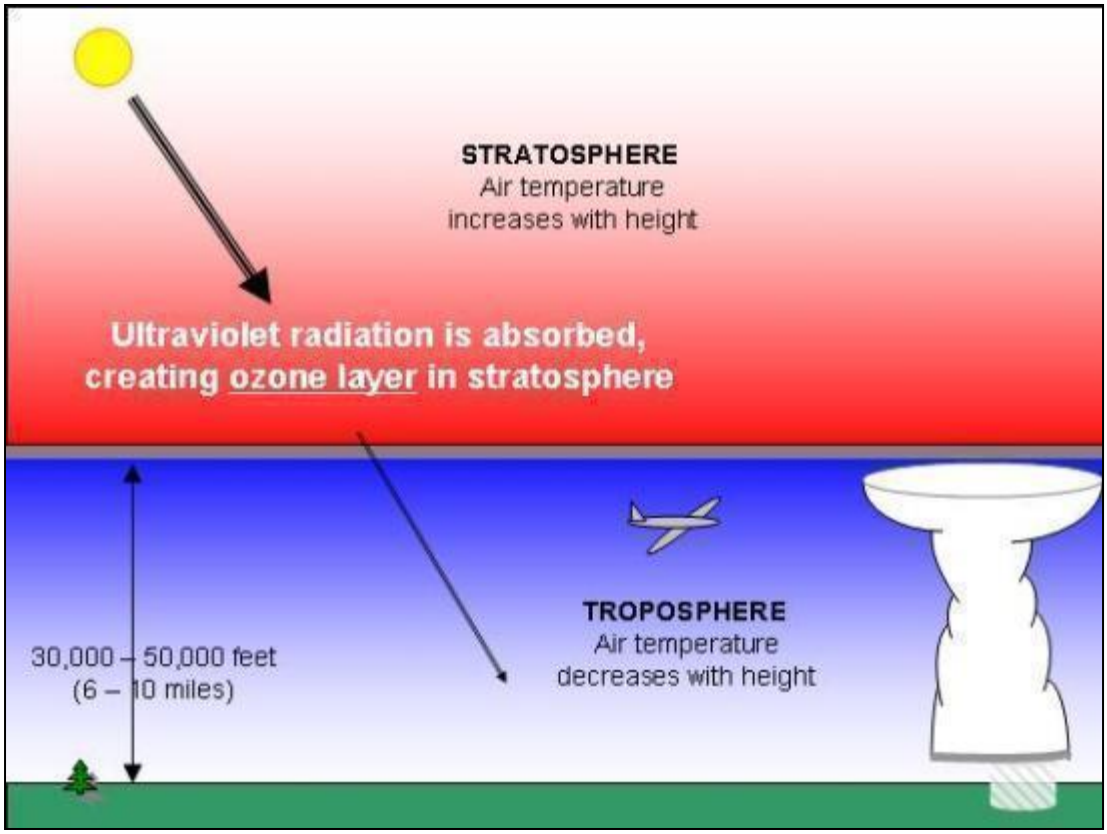

Fig.1 (b) Ozone layer in the Stratosphere

Generation of Ozone in the Stratosphere: Oxygen gas (O_2) is present in the atmosphere. High energy or shorter wavelength UV light (*hv*) collides with the oxygen molecule (O_2), causing it to split into two oxygen atoms. These atoms are unstable, and they prefer being "bound" to something else. The free oxygen atoms then smash into other molecules of oxygen, forming ozone (O_3).

$$O_2 + h\nu \rightarrow O_1 + O_1$$

$$O_{1\ (atom)} + O_{2\ (Oxygen\ gas)} \rightarrow O_{3\ (Ozone)}$$

The overall reaction between oxygen and ozone formation is:

$$3\ O_2 \rightarrow 2\ O_3$$

The ozone is destroyed in the process that protects us from UV-B and UV-C rays emitted by the Sun. When ozone (O_3) absorbs UV light *(hv)*, it will split the molecule into one free oxygen atom (O_1) and one molecule of oxygen gas (O_2). Thus, absorption of UV-B and UV-C leads to the destruction of ozone

$$O_{3\ (Ozone)} + h\nu \rightarrow O_{1\ (atom)} + O_{2\ (Oxygen\ gas)}$$

Ozone is valuable to us because it absorbs harmful UV radiation during its destruction process (fig.2 (a)). A dynamic equilibrium is established in these reactions. The ozone concentration varies due to the amount of radiation of light received from the sun.

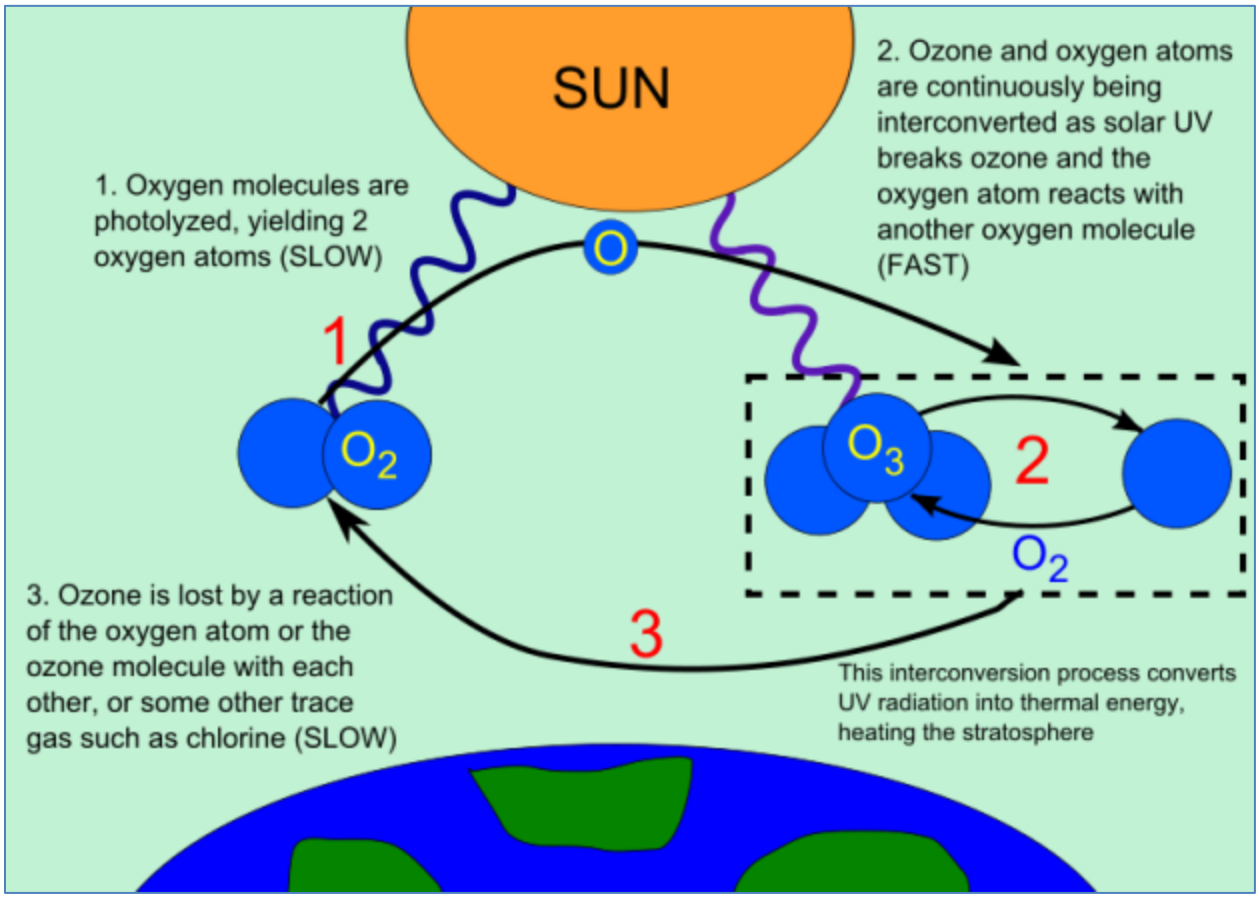

Fig.2 (a) Generation of ozone in the presence of UV light in stratosphere

(Source: http://nanopatentsandinnovations.blogspot.com/2012/07/serious-and-wholly-unexpected-ozone.html)

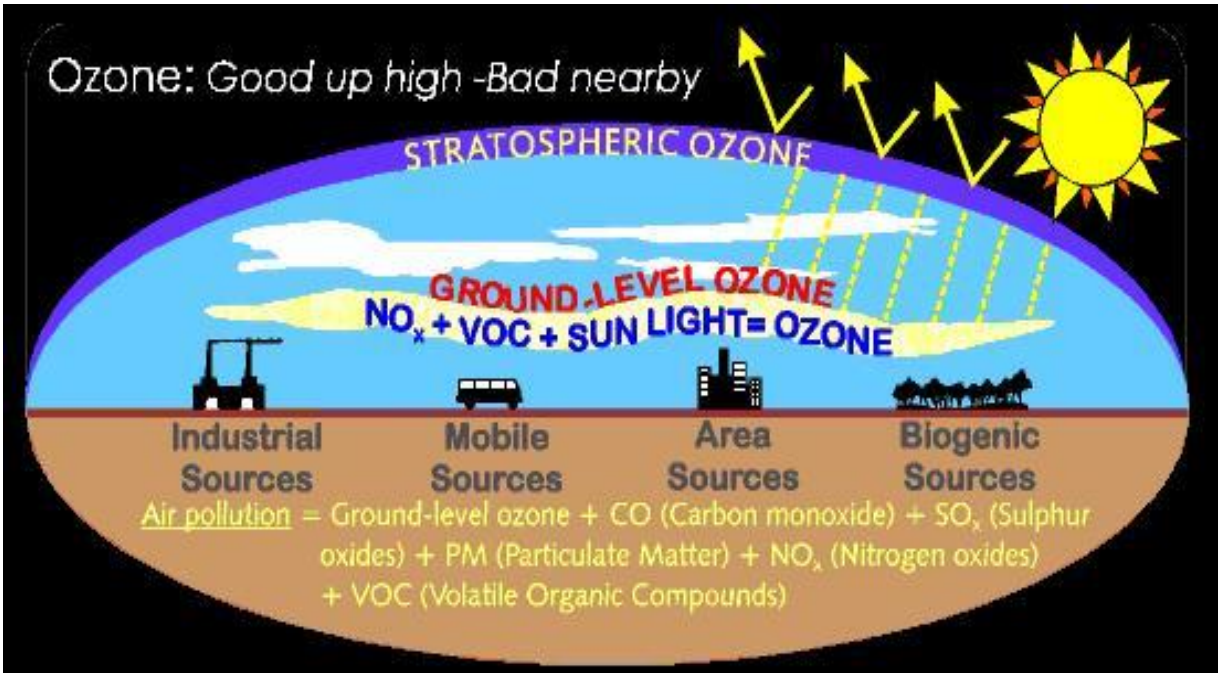

Fig. 2(b) Good ozone and bad ozone

Generation of Ozone in the Troposphere: Ozone in the troposphere is bad. It creates the respiratory problem, destroys polymers and reduces the plant growth. This ozone is contributing to the smog and greenhouse gases created by human activities, which is shown in fig.2 (b). Ozone close to the ground surface does not exist in high enough concentrations to shield us from UV light.

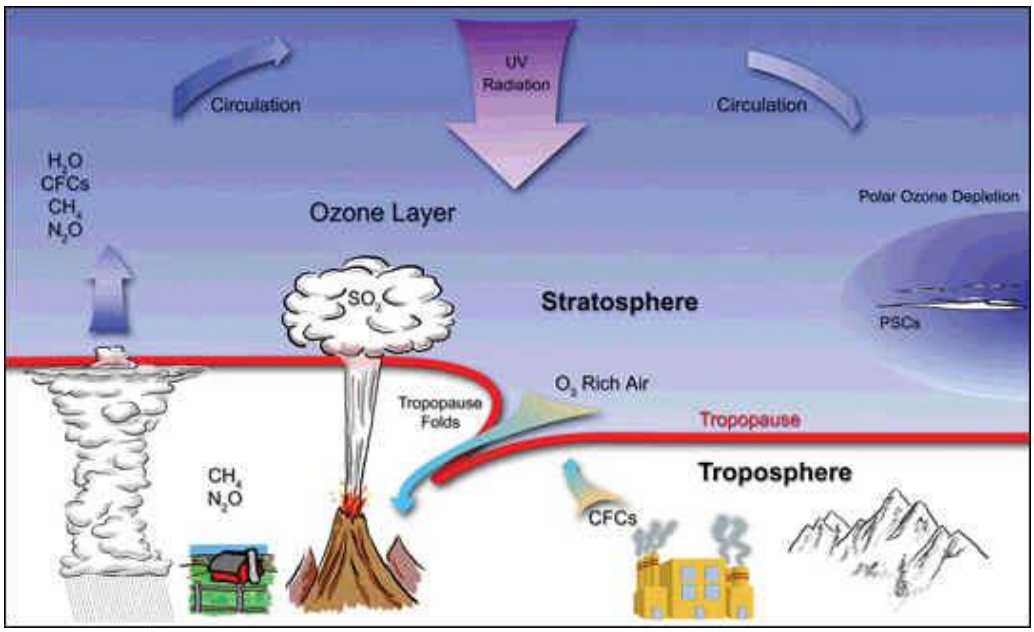

Courtesy: http://www.theozonehole.com/ozonedestruction.htm

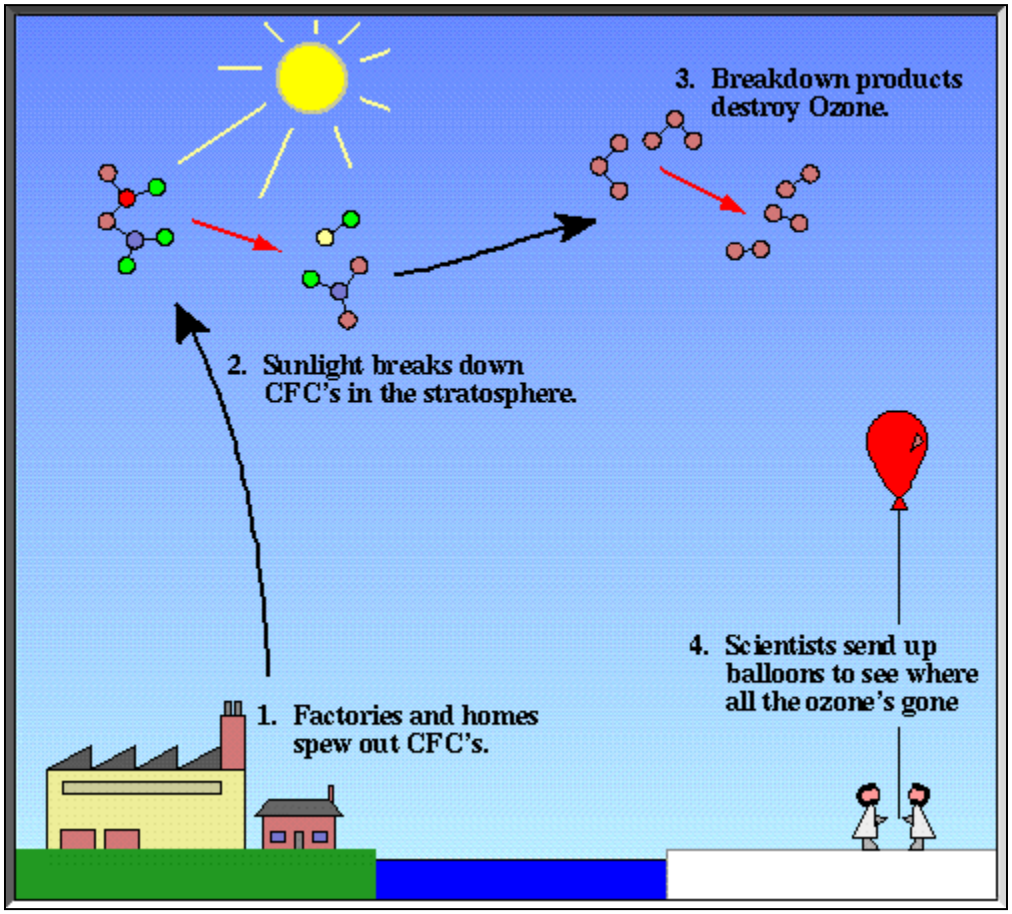

Fig.2 (c) Life cycle of the chlorofluorocarbons (CFCs)

Pollutant gases, particularly, chlorine and bromine compounds in the atmosphere are responsible to cause the ozone depletion, which is mainly observed in the `ozone hole' over Antarctica and over the North Pole. Most of the chlorine, and nearly half of the bromine in the stratosphere, where most of the depletion has been observed, comes from human activities. Fig. 2 (c) shows a schematic illustrating the life cycle of the chlorofluorocarbons (CFCs); how they are transported up into the upper stratosphere/lower mesosphere, how sunlight breaks down the compounds and then how their breakdown products descend into the polar vortex.

HASP-NASA provided a platform for 12 small payloads and 4 large payloads. The maximum mass limit for a large payload was 20 kg and 3 kg for a small payload. UND and UNF jointly had one small payload. UNF's responsibility was to provide the gas sensors system, payload body and data analysis, while UND's responsibility was to provide the microcontroller circuit, software, and electronic communication circuits. The HASP had an onboard computer, power supply batteries, GPS, video camera, and communication link for all payloads. During the July 28 to August 3, 2013, the UND and UNF team met at the NASA-Columbia Scientific Balloon Facility (CSBF) in Palestine, Texas for the integration of the sensors and electronic circuits that

made a complete UND-UNF payload. The payload was then integrated with the HASP platform. The UND-UNF payload successfully passed all required thermal vacuum tests and certified for the flight. Then, the HASP2013 flight was launched successfully by NASA-CSBF on Monday, September 2, 2013 from Fort Sumner, New Mexico. The flight duration was about 10:30 hours. During the flight, the UNF ozone sensors array worked and detected ozone in the stratosphere. The payload sent out a data files during the flight without any problem. After the termination of the balloon flight, the payload landed safely on the ground using a parachute. Then, the payload was recovered. The technical details, pictures and science results of this flight are highlighted in this report.

Fabrication of Nanocrystalline Ozone Gas Sensors

Ozone sensors were fabricated by UNF team at Dr. Patel's sensors laboratory at the UNF. Fig.3 show (a) and(b) shows thermal vacumm deposiiton system and electron beam deposition system, respectively, were used to fabricate nanocrsyaline nanocomposite thin film gas sensors for the detection of ozone gas.

Fig. 3 (a) Thermal vacuum depsoition system and (b) electron beam depsoition system

Fig. 4(a) shows the top view of one typical low magnification scanning electron microscope image of the Indium Tin Oxide (ITO) thin film gas sensor having two gold electrodes for external electrical contacts.

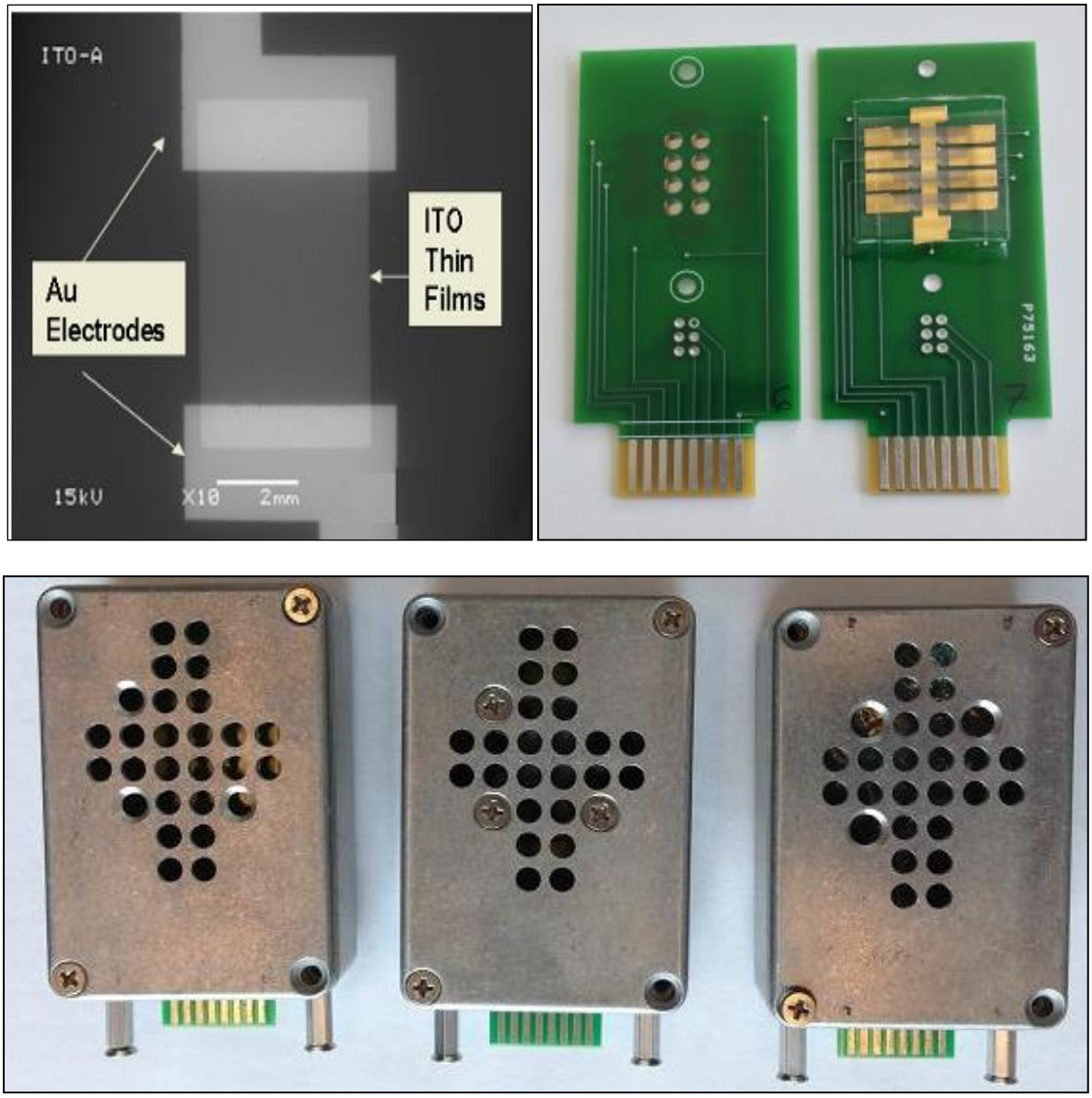

Fig.4 (a) Scanning electron microscope image of top view of one ITO gas sensor, (b) Top and bottom view of 8 gas sensor array interface with the printed circuit board (PCB) (UNF Patent pending) and (c) Three sensors boxes # 1, 3 and 4.

Fig. 4 (b) shows a typical array of 8 ITO thin film gas sensors fabricated on an approximately 2.5cm x 2.5cm ultra cleaned glass slide. The glass slides were throughlly cleaned by the ultrasonic cleaner, detergent, solvant and baked in the ovan. The interface of the cicuit board to the array is also shown in. Fig. 4(b). Three types of sensor array boxes were fabicated as shown in Fig. 4(c). Each type of sensor array was mounted in a separate box. In addition to the sensors box for the payload, two backup sensors boxes were fabricated. All sensors boxes were

calibrated at UNF by UNF students team members (Rebecca, Jason, and Ken) at different time period (Fig. 4(d)) and then tested in the thermal vacuum test chamber at CSBF, Palestine, TX.

Box #1 sensors are nanocrystalline ITO thin film deposited on glass.

Box #3 sensors are nanocomposite of ZnO + ITO thin films deposited on glass.

Box #4 sensors are nanocomposite of WO_3 + ITO thin films deposited on glass.

Note: There is no Box#2.

Fig. 4(d) Rebecca Polo, student team member of UNF with sensor arrays PCBs

Fig. 5 (a) shows the picture of housing for the UNF sensors, consisting of an array of 8 gas sensors interfaced with a printed circuit board (PCB), flexible Kapton heater (MINCO make HK 5573R30.0 L12BU), temperature sensor (Analog Device TMP36), electrical fan (SUNON, MC25060V2-0000-A99, DC 5V, 0.38W) and a 16 wires flat cable. One end of flat cable has a female card edge connector to connect sensor PCB (Make: 3M, MCS16K-ND), while other end has 16 pin female to connect microcontroller PCB.

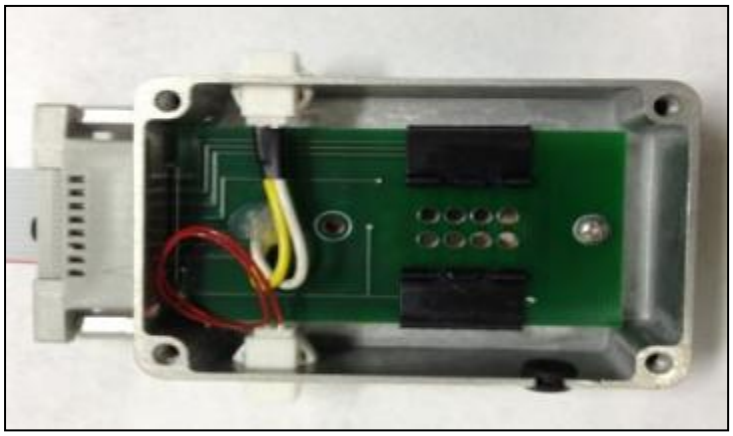

Fig.5 (a) Inner view of UNF Ozone sensors box

The pin information of sensor PCB and connector are shown in fig. 5(b) and (c), respectively.

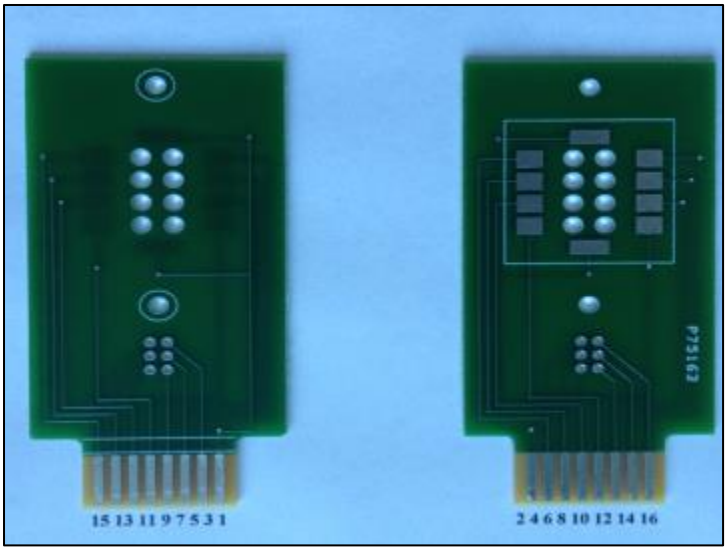

Fig.5 (b) Pin numbers of sensors PCB

Pin number per connector datasheet							
1	3	5	7	9	11	13	15
Common	Temp Sensor	Temp Sensor	Temp Sensor	Gas Sensor	Gas Sensor	Gas Sensor	Gas Sensor
Open	Gas Sensor	Gas Sensor	Gas Sensor	Gas Sensor	Light Sensor	Light Sensor	Pin not used
2	4	6	8	10	12	14	16
Pin number per connector datasheet							

Fig.5 (c) Pin information for connection of 16 pins female card edge connector with sensors PCB

Working Principle of Sensors

Interaction of oxidizing gas on surface of n-type ITO thin film sensor

Upon adsorption of charge accepting molecules at the vacancy sites, namely from oxidizing gases such as ozone (O_3), these electrons are effectively depleted from the conduction band of ITO. This leads to an increase in the electrical resistance of n-type ITO.

For ozone gas:

Oxygen vacancy (V) + Ozone (O_3) →Lattice Oxygen site (O_o) + O_2

Vacancies can be filled by the reaction with ozone. Filled vacancies are effectively electron traps and as a consequence the resistance of the sensor increases upon reaction with ozone.

Interaction of reducing gas on surface of n-type ITO thin film sensor

Oxygen vacancies on ITO surfaces are electrically and chemically active. These vacancies function as n-type donors decreasing the electrical resistivity of ITO. Reducing gases such as CO, H_2 and alcohol vapors result in detectable decreases in the electrical resistance of n-type ITO.

For methanol:

CH_3OH (methanol) + O^- (chemisorbed ion on surface of ITO)

→ HCOH (Formaldehyde) + H_2O (water) + e^- (electron)

Vapors come in contact with the surface and react with chemisorbed oxygen ions O- or O^{2-} and re-inject electrons into the conduction band.

In summary, the electrical resistance of ITO increases in the presence of oxidizing gases such as ozone. Upon adsorption of the charge accepting molecules at the vacancy sites, namely oxidizing gases such as ozone, electrons are effectively depleted from the conduction band, leading to an increase in the electrical resistance of n-type ITO.

Calibration of ITO Sensors

The ITO sensors array was first tested and calibrated in the test chamber at UNF. The test chamber was adjusted to the identical coonditions of temperature and pressure as in the startosphere. Fig. 6(a) and (b) shows the pictures of ozone generator and detector used for the calibration of sensors. An ozone gnerator (Ozone Solutions, Model# OMZ-3400) was used as the source of ozone, which generated 0 to 12 ppm ozone gas. A digital ozone detector(Eco Sensors, Inc., Model:A-21ZX) was used to measure the concentration of ozone in part per million (ppm). The Keithley digital multimeters and electrometers attached with comoputer having LabView program wereused for the measurements of the ITO sensor's resistance.

Fig.6(a) Ozone generator and (b) digital ozone detector

All the 24 sensors of sensors box was calibrated simulataneously under indetical conditions of pressure, temepratue and concnetration of ozone in the test chamber. The sensors were calibrated with ozone gas in the range of 0.02 to about 10.00 ppm in the test chamber in the same run. The usual variation of ozone in the stratosphere is about 3.0 to 8.5 ppm. The measured data fit linearly and trendline equations for each plot were determined

Figs.7 (a) to (h) show the calibration plots ozone sensors **Box#1 having sensors # S1-1 to S1-8**. These sensors were made of nanocrystalline ITO thin film gas sensors fabricated on the glass.

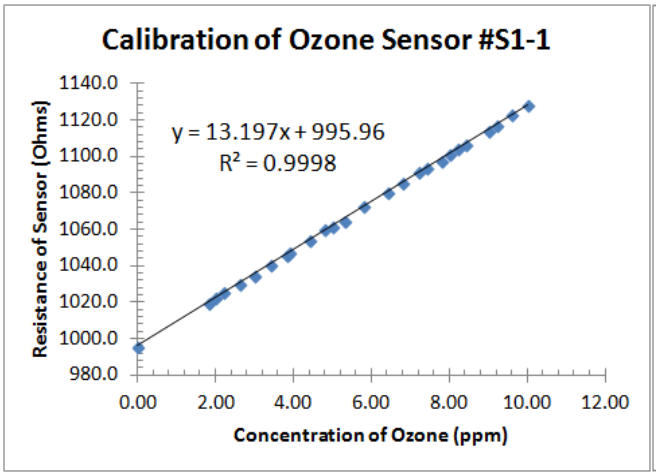

Fig.7 (a)

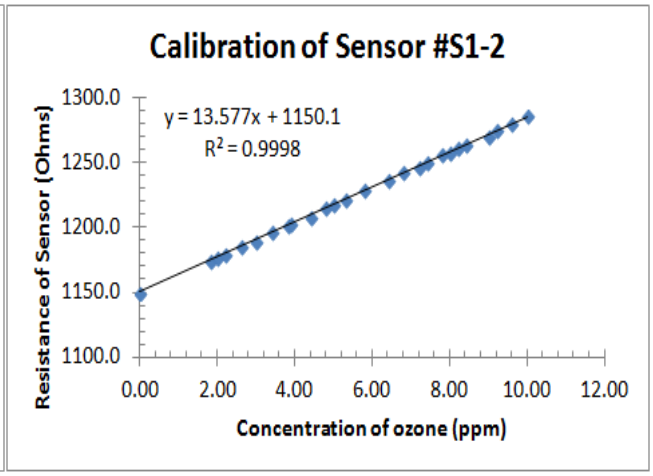

Fig.7 (b)

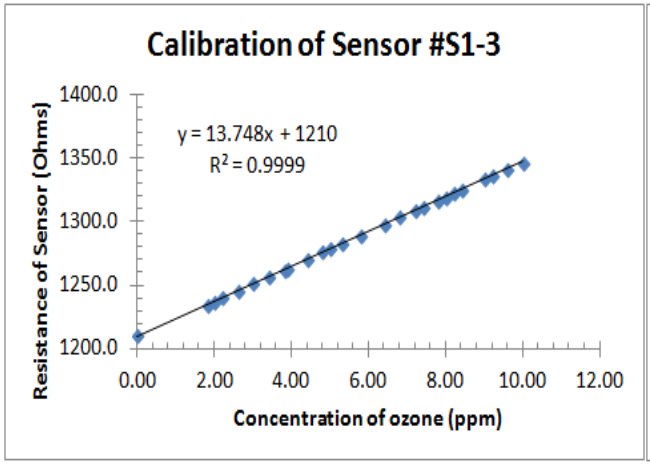

Fig.7 (c)

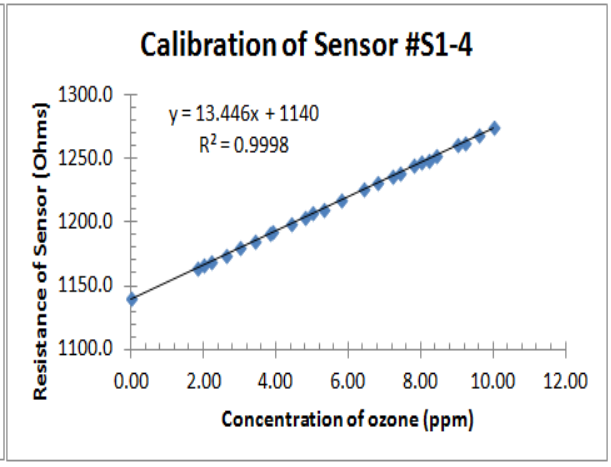

Fig.7 (d)

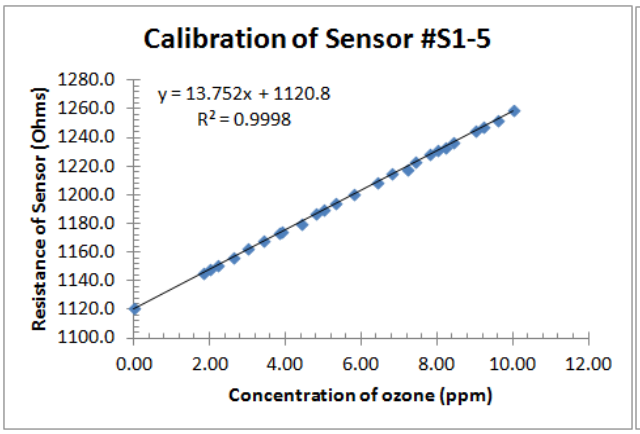

Fig.7 (e)

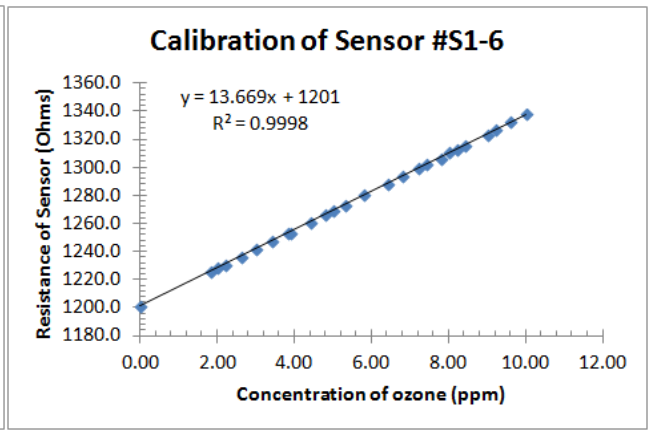

Fig.7 (f)

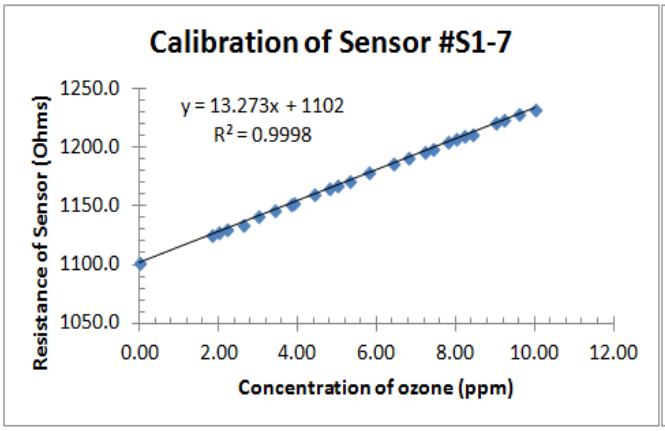

Fig.7 (g)

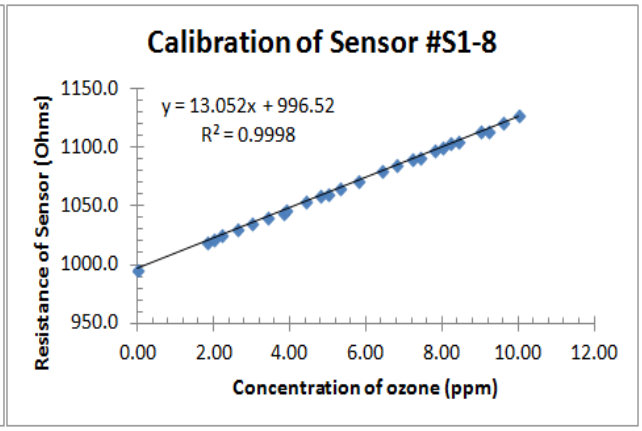

Fig.7 (h)

Figs.7 (a) to (h) show the calibration plots ozone sensors Box#1 having sensors # S1-1 to S1-8. These sensors were made of nanocrystalline ITO thin film gas sensors fabricated on the glass.

Figs.7 (i) to (p) show the calibration plots ozone sensors **Box#3 having sensors # S3-1 to S3-8**. These sensors were made of nanocomposite of ZnO + ITO thin film gas sensors fabricated on the glass.

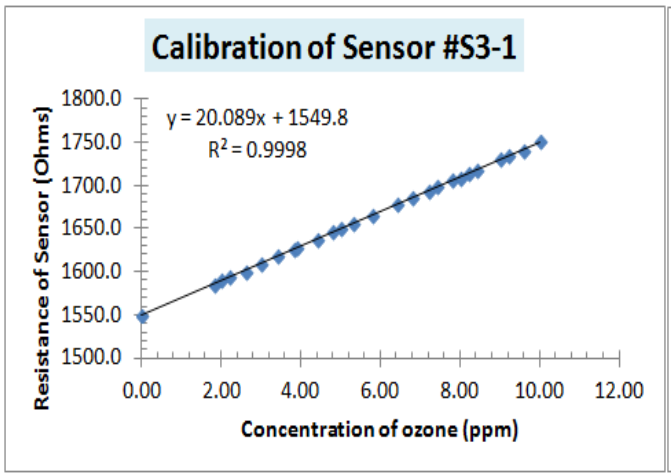

Fig.7 (i)

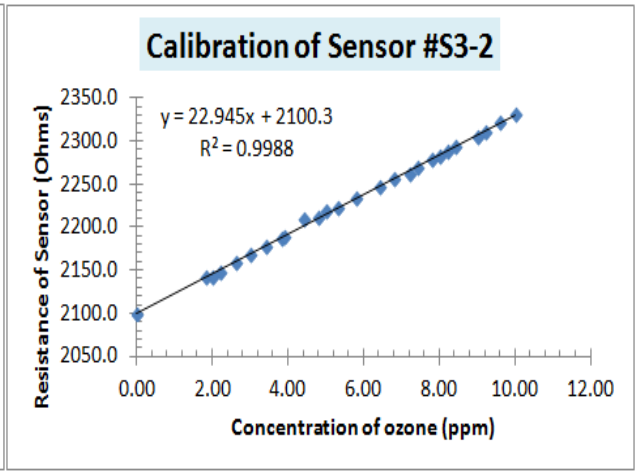

Fig (j)

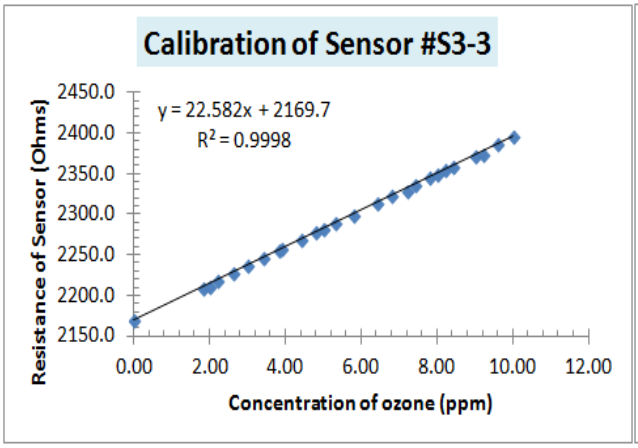

Fig.7 (k)

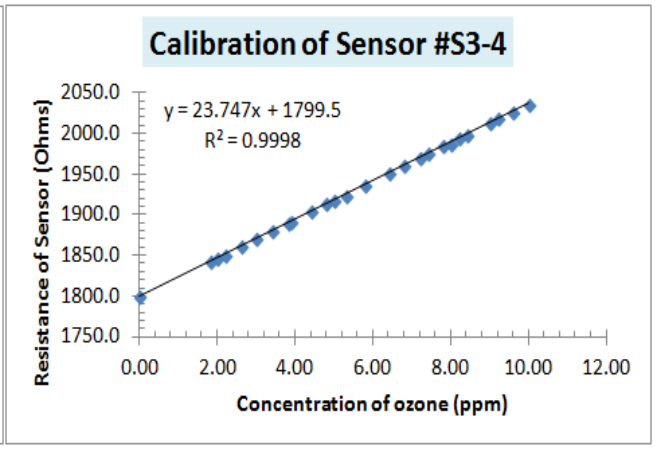

Fig.7 (l)

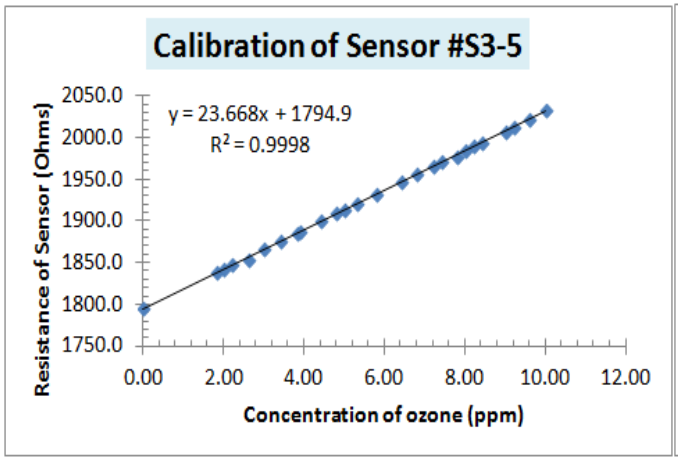

Fig.7 (m)

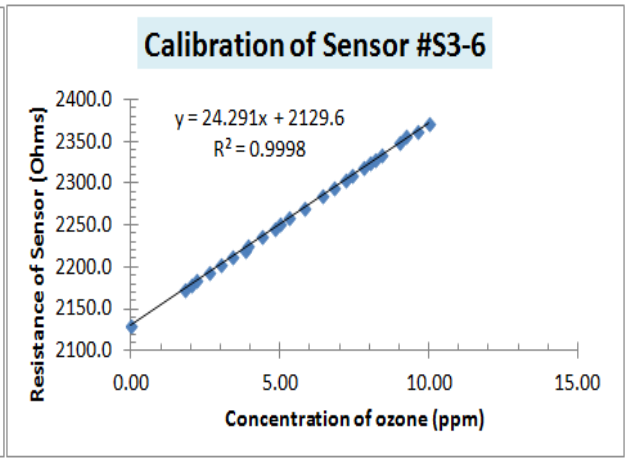

Fig.7 (n)

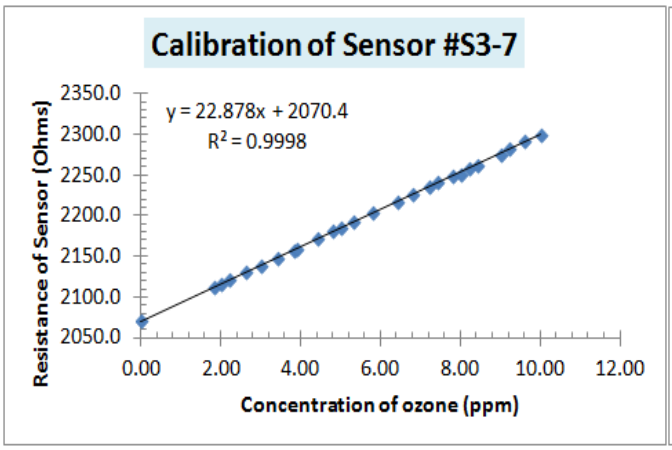

Fig.7 (o)

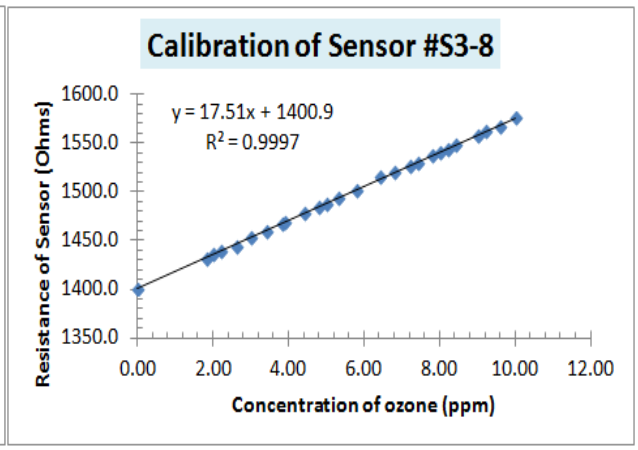

Fig.7 (p)

Figs.7 (i) to (p) show the calibration plots ozone sensors Box#2 having sensors # S3-1 to S3-8. These sensors were made of nanocomposite of ZnO and ITO thin film gas sensors fabricated on the glass.

The calibration plots ozone sensors Box#4 having sensors # S4-1 to S4-8 were also performed. The plots are not presented here. These sensors were made of nanocomposite of WO_3 and ITO thin film gas sensors fabricated on the glass.

All sensors were calibrated at three different times and showed nearly the same nature of response each time. Small variations in the slope and y-intercept values were observed due to experimental error.

Fabrication of Payload Body

The main features of our newly designed payload body are easy to open and close payload, easy access of PCB and sensor boxes, low rate of outgassing under low pressure, better stability with thermal and impact, and reusable. The following parts were procured for payload body from supplier www.onlinemetals.com.

Name	Size	Purpose
Aluminum Extruded Square Tube Part #6063-T52	height 11” w x d: 6” x6” wall thickness: 0.125”	Payload body
Aluminum Sheet Part#3003-H14	6” X 6” Thickness:1/8”	Top lid
Aluminum Finished Rectangles Part#2024-T351	0.625”X1”	Internal support of payload with base plate and lid

Ken Emanuel made design drawing and fabricated payload body in the workshop of Department of Engineering of UNF. Design diagrams are shown in Fig. 8 (a) to (k).

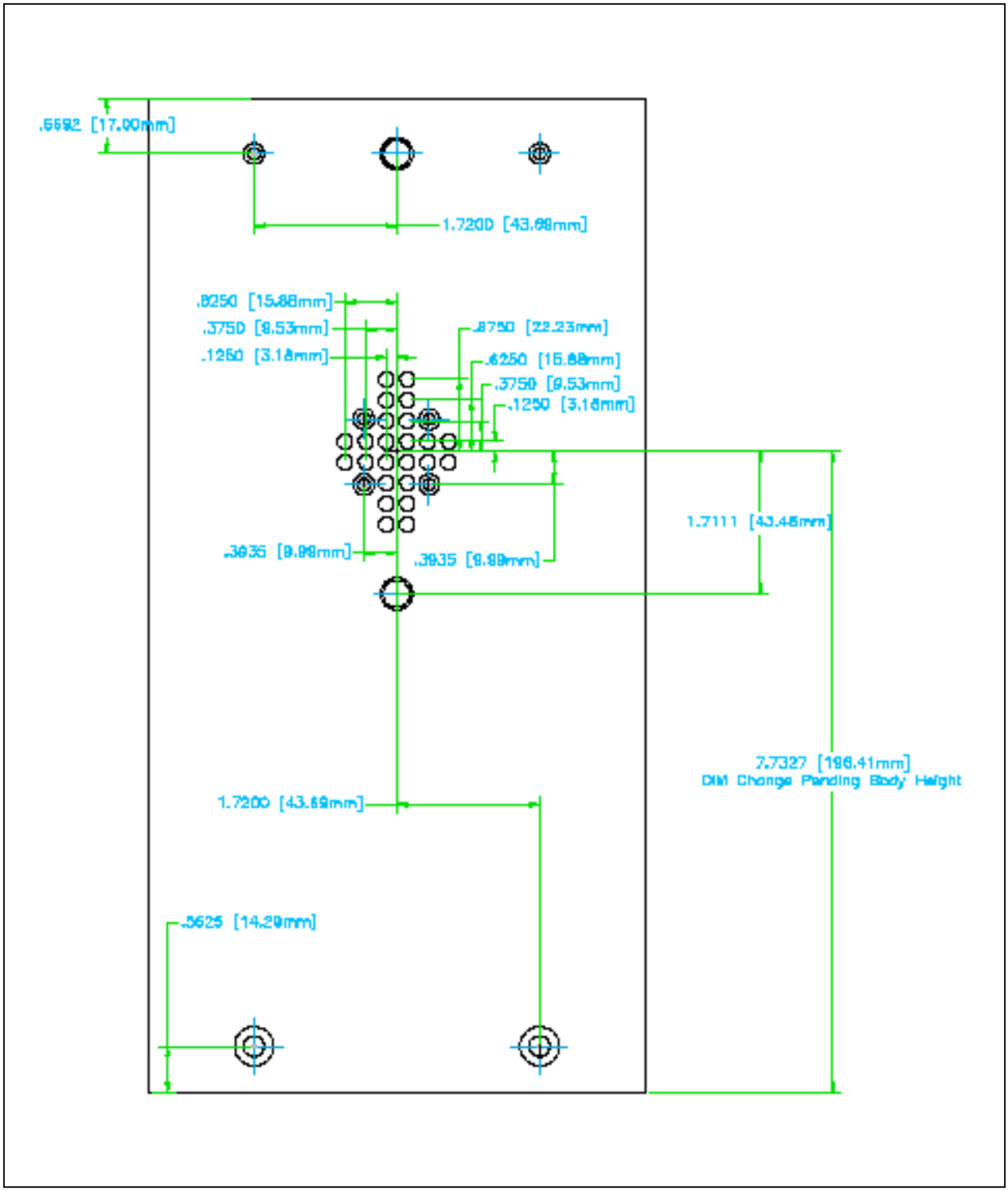

Fig.8 (a) Design for holes on two opposite sides (Side #1 and 3) of payload body

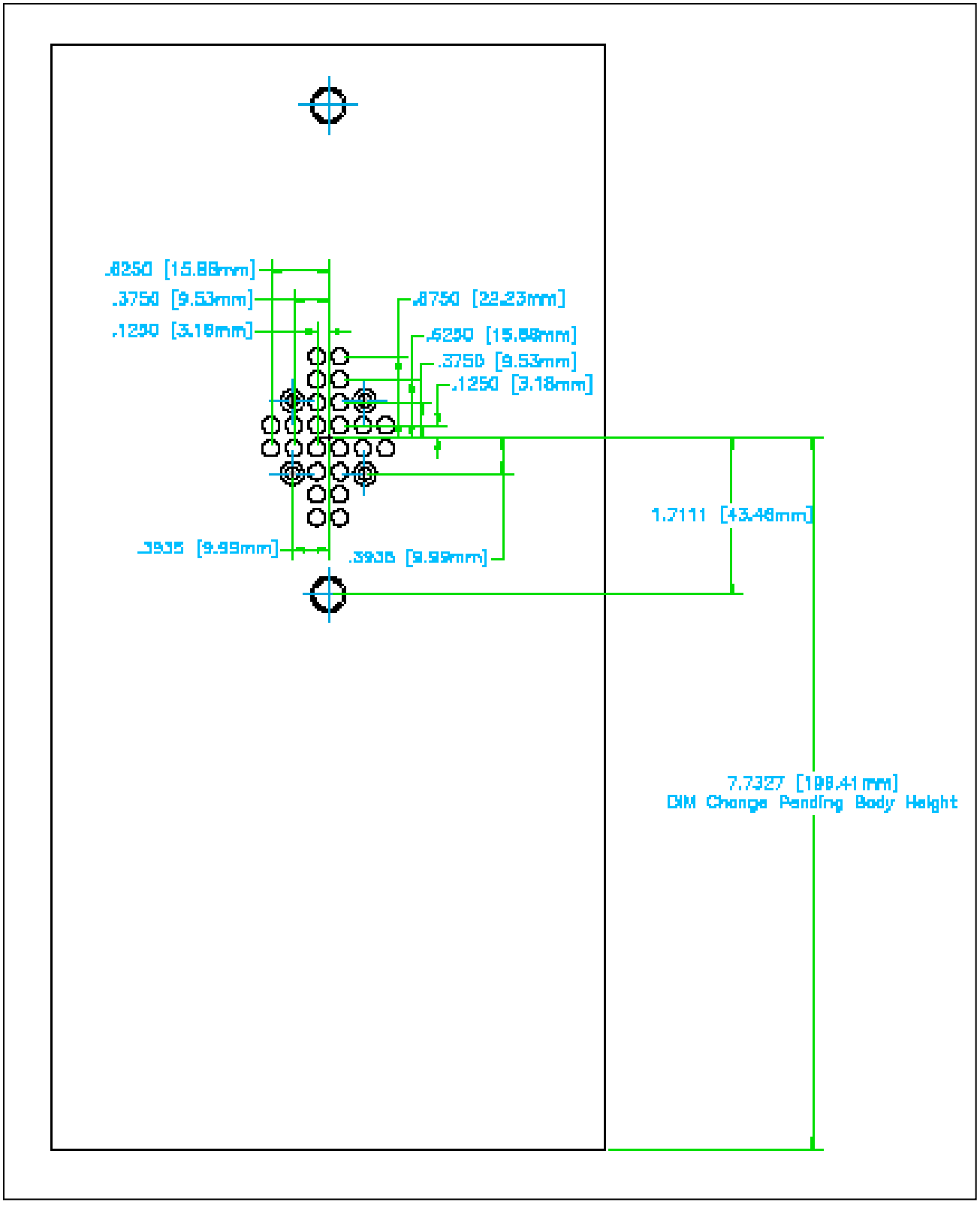

Fig.8 (b) Design for holes on Side # 2 of payload body

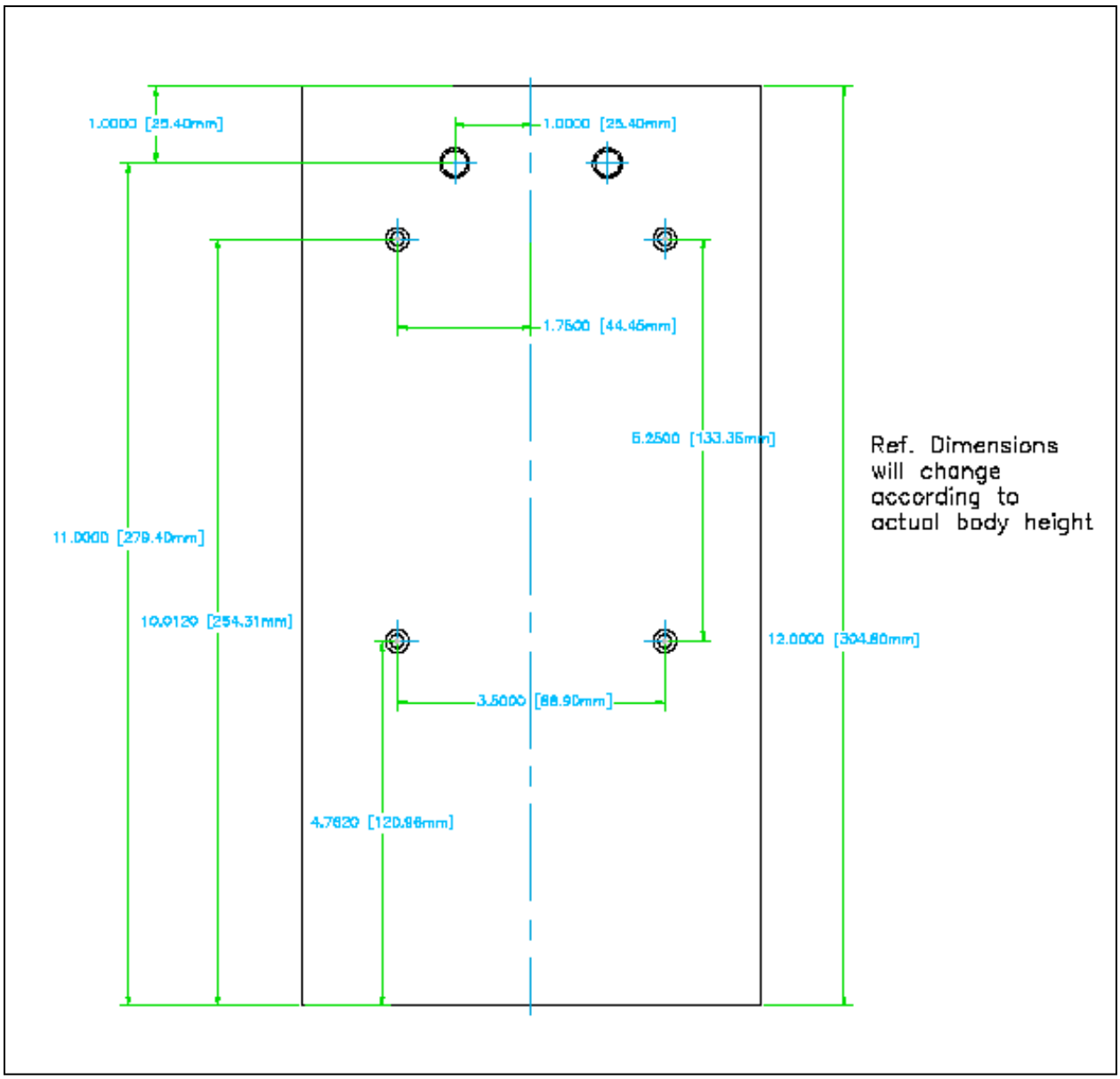

Fig.8 (c) Design for holes on fourth side (Side #4) of payload body for mounting microcontroller PCB

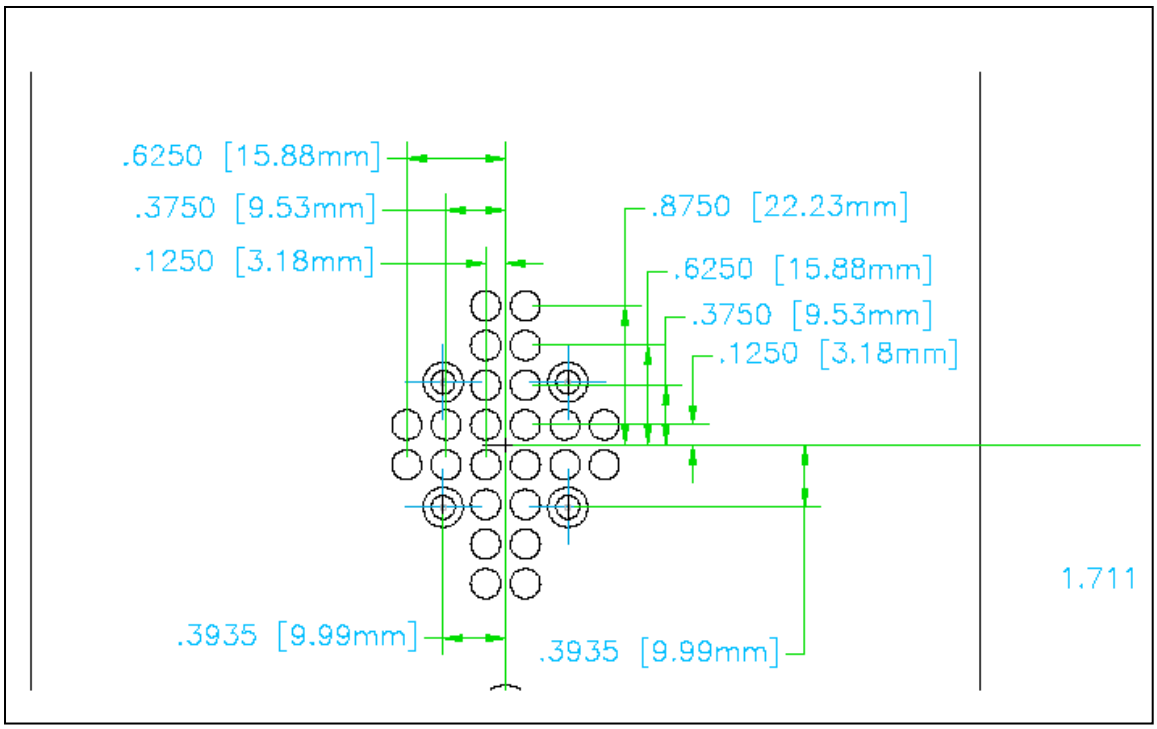

Fig.8 (d) Details of design for holes on three sides of payload body for fan and air inlet

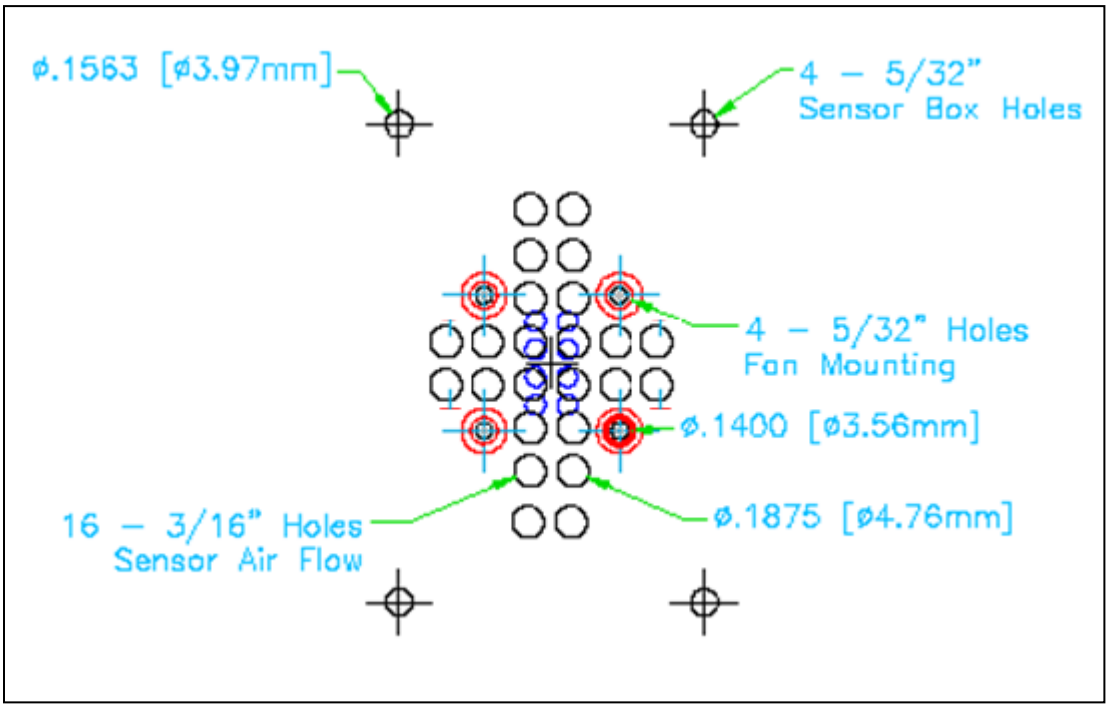

Fig.8 (e) Details of design for holes on three sides of payload body and sensor box

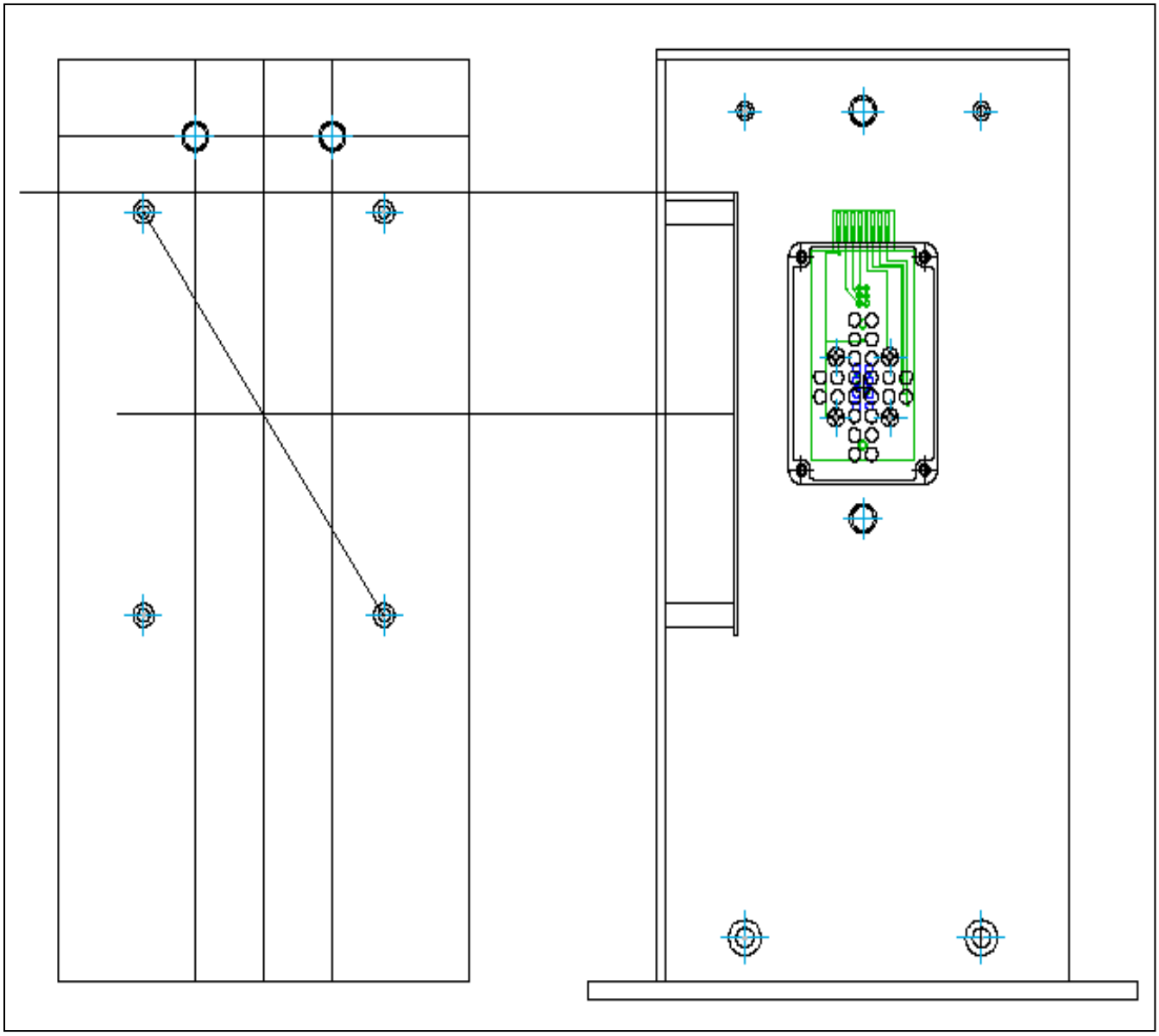

Fig.8 (f) Design for holes on payload body for mounting microcontroller PCB and sensor box

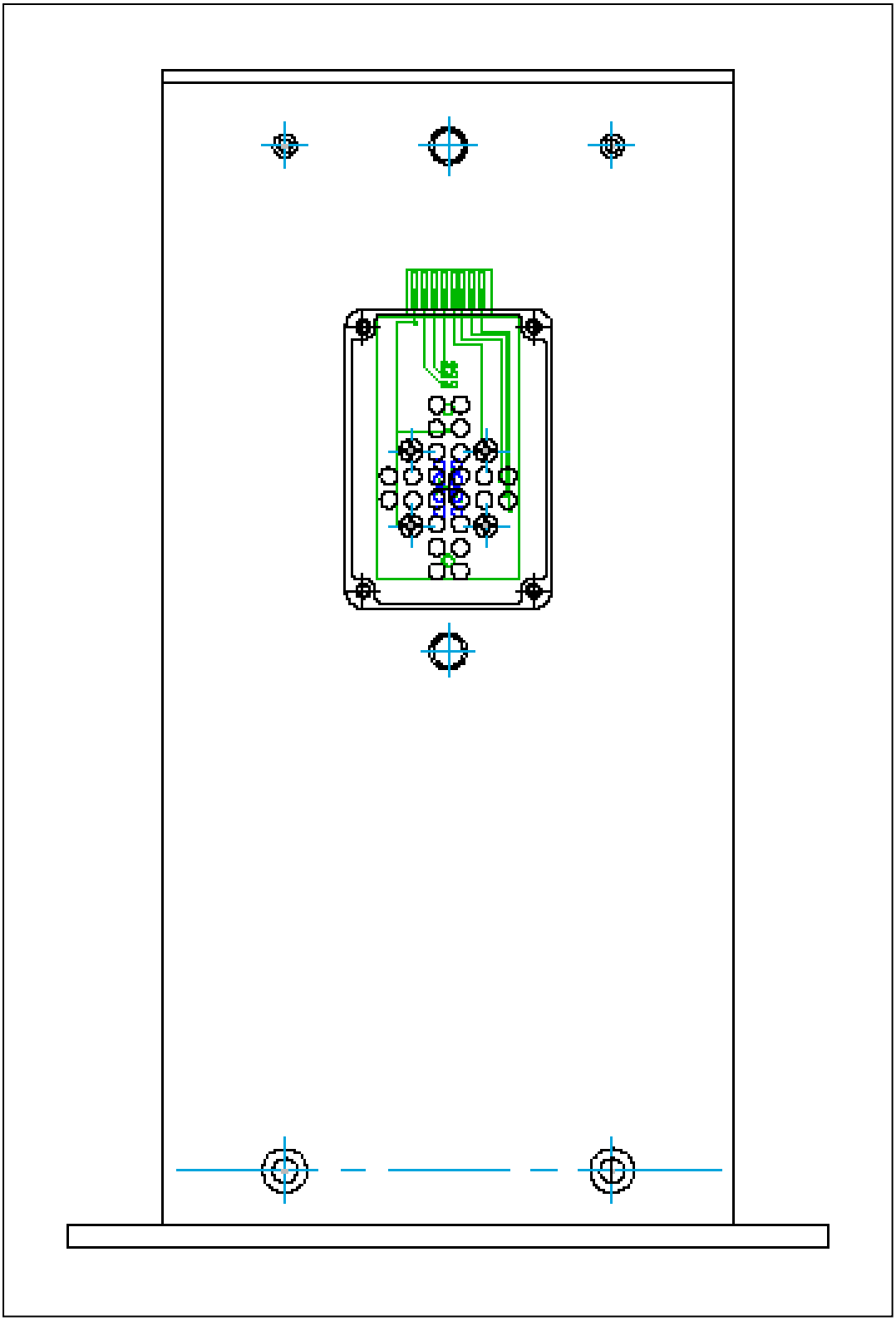

Fig.8 (g) Design for holes on payload body for mounting of sensor box, LED, Light sensor and HASP mounting plate

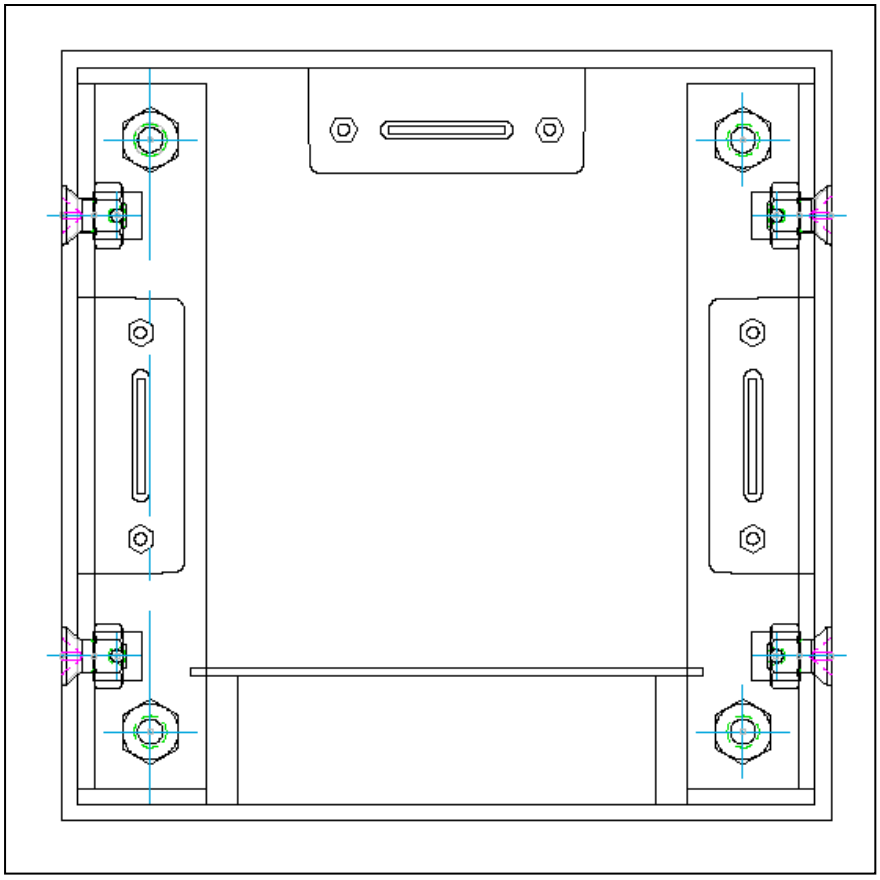

Fig.8 (h) Top view of payload

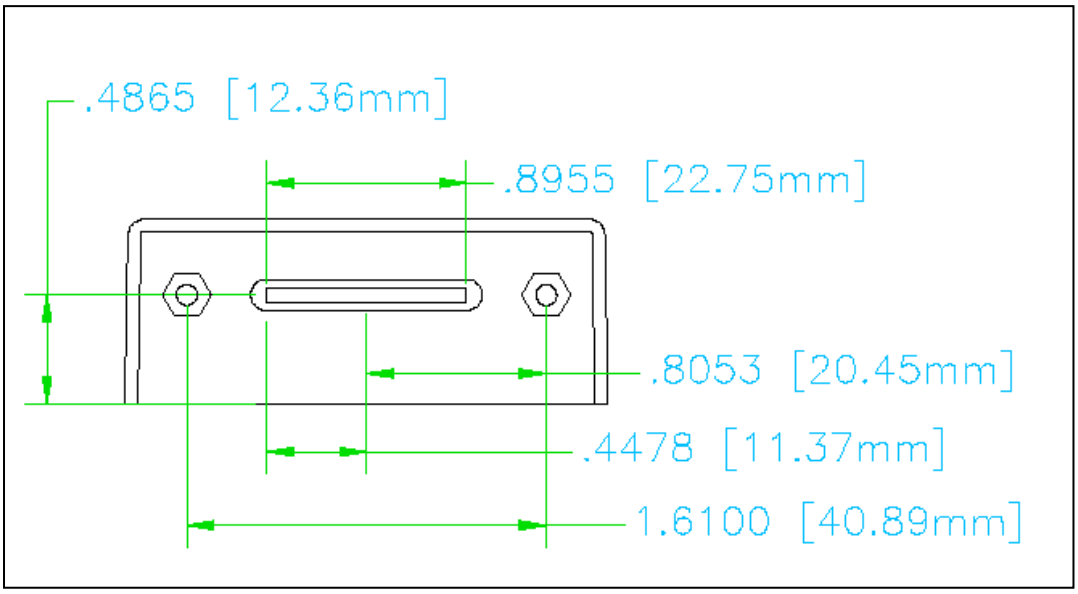

Fig.8 (i) Design for standoff and PCB slot in the sensor box

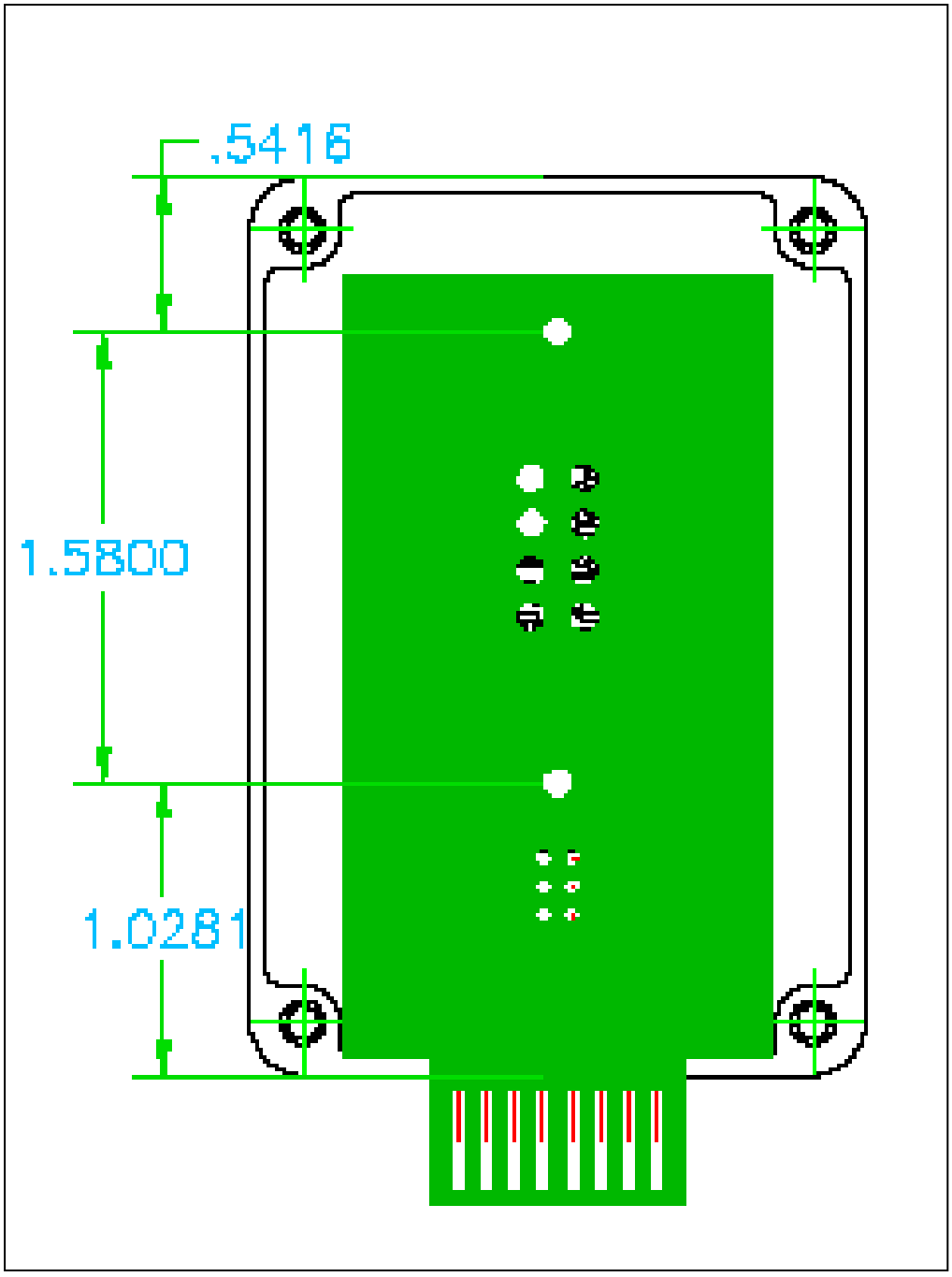

Fig.8 (j) Design for standoff to mount sensor SPCB in the box

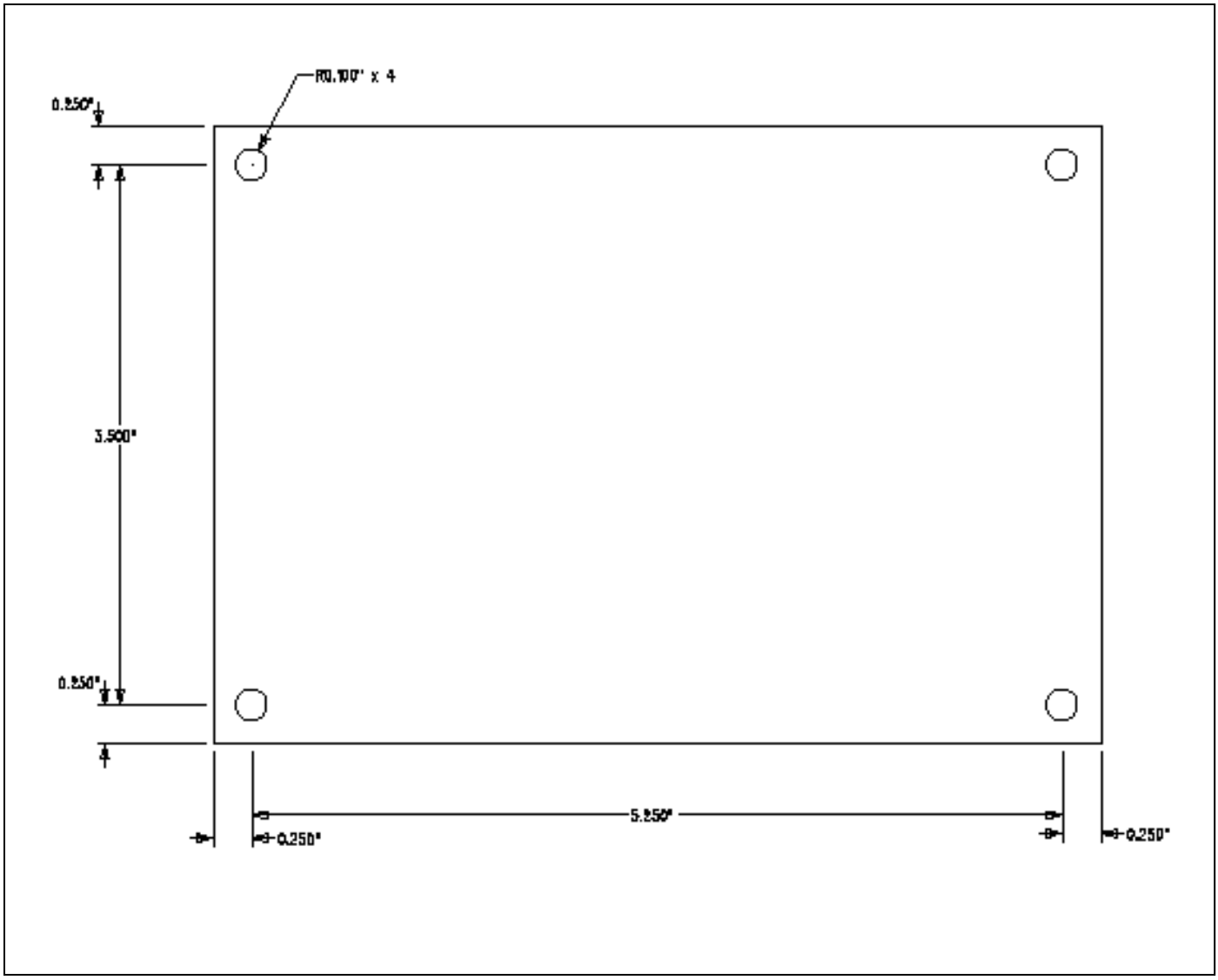

Fig.8 (k) Design for hole of the microco0ntroller PCB

The pictures of the payload body are shown in fig.8 (l) and (m). The dimensions of payload were 296mm x 149mm x 149mm, which were within the requirement of being less than 300mm x 150mm x 150mm.

.

Fig.8 (l) and (m) Payload body structure

Fig.9 Weight budget of various parts of the payload

Fig.9 shows weighing of payload using the digital balance. The total mass of payload including its base plate was 3.210 kg, which was less than the limit of 3.00 kg + 0.50 kg mass of base plate (total 3.5 kg).

Cirucit diagrams

Jonathan Snarr (UND) developed the micorcontroller circuits. The block diagram of circuit is shown in fig. 10 (a), while several sections of circuits are shown in fig. 10 (b) to (h). Two identical microcontroller PCBs were fabricated. The picture of PCB is shown in fig.10 (i). Two identical PCBs were fabricated. One PCB was used for the payload, while for other PCB was used to stimulate software and backup.

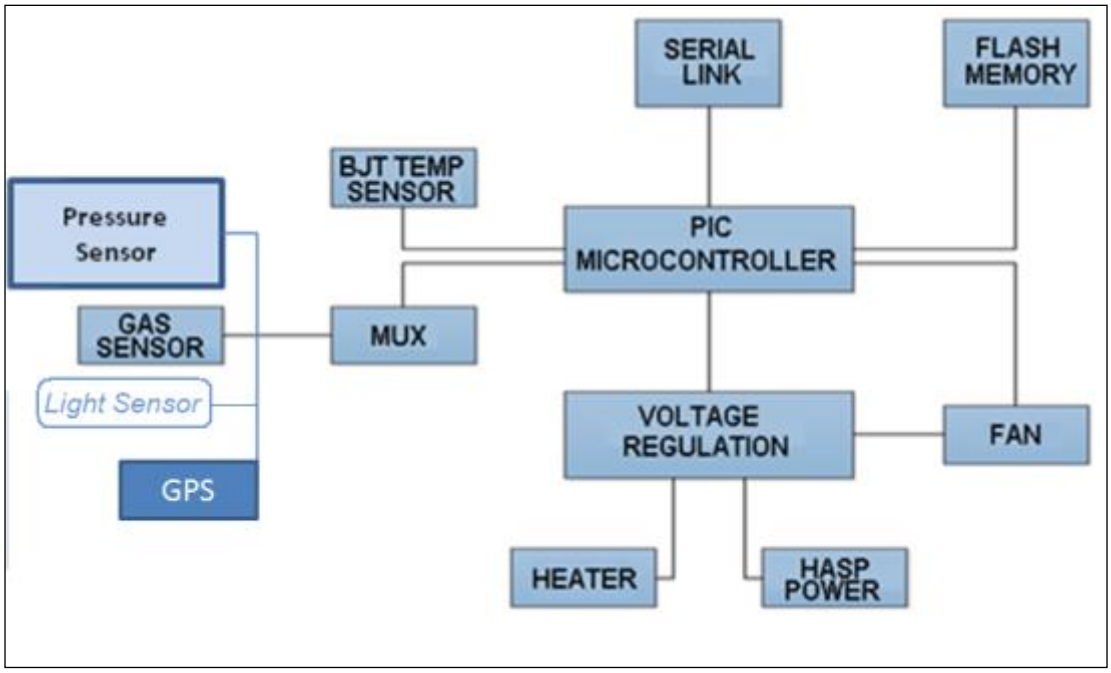

Fig. 10(a) Block diagram of payload ciruct

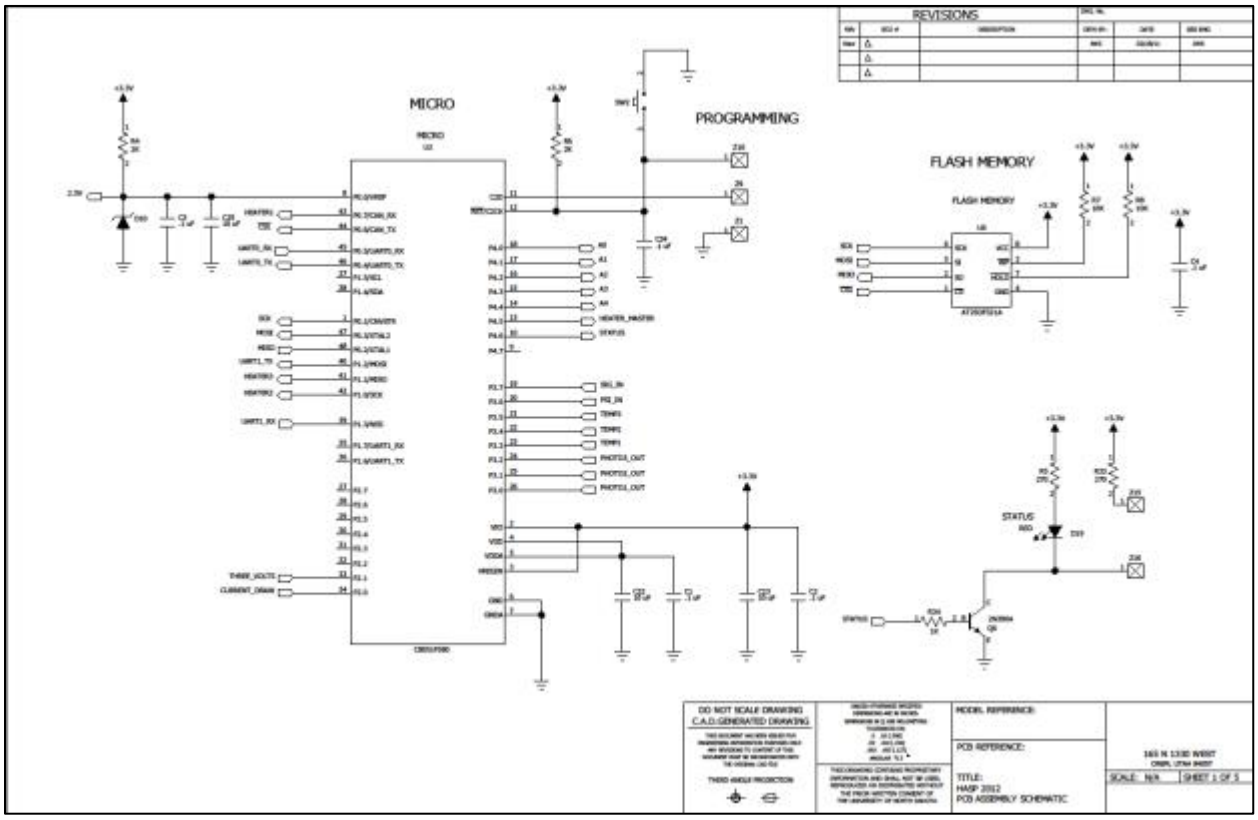

Fig. 10 (b) Circuit for microcontroller and flash memory

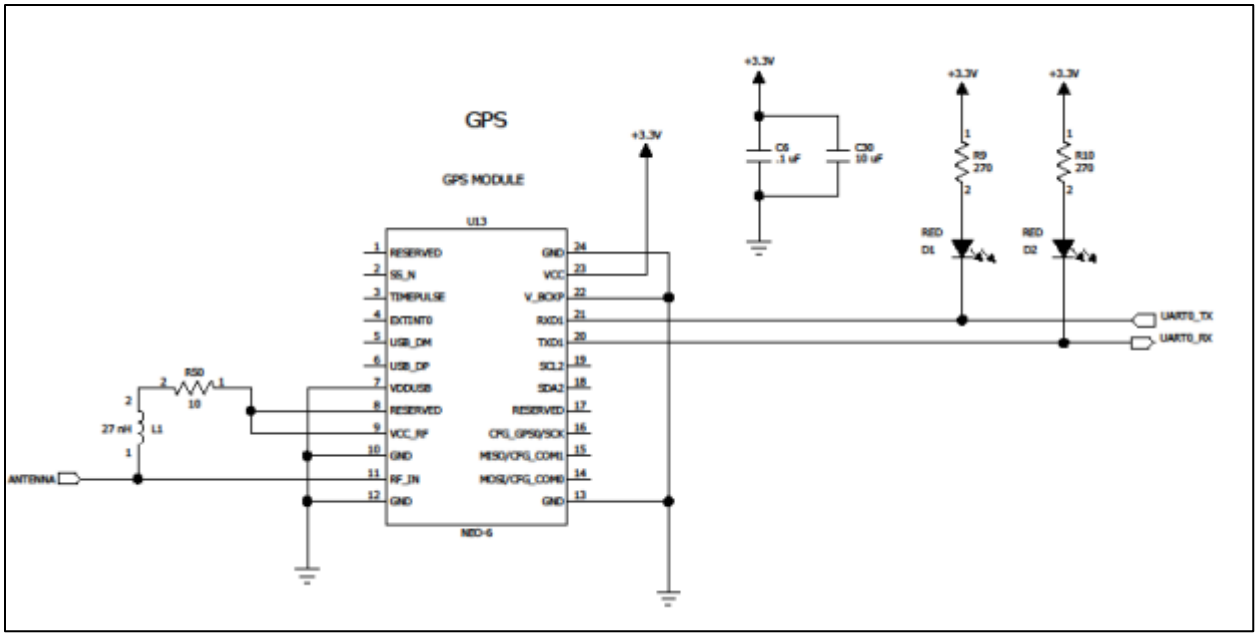

Fig. 10 (c) Circuit for GPS

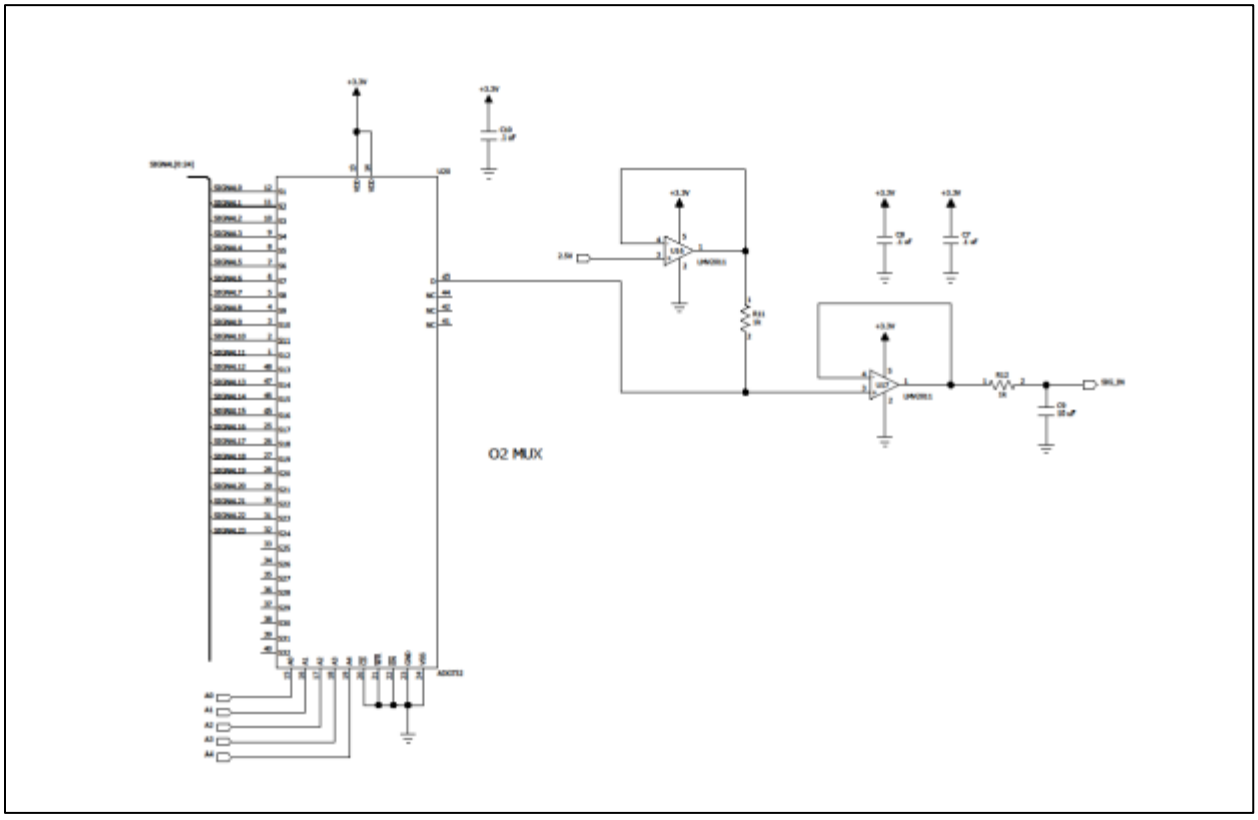

Fig. 10 (d) Multiplexer circuit

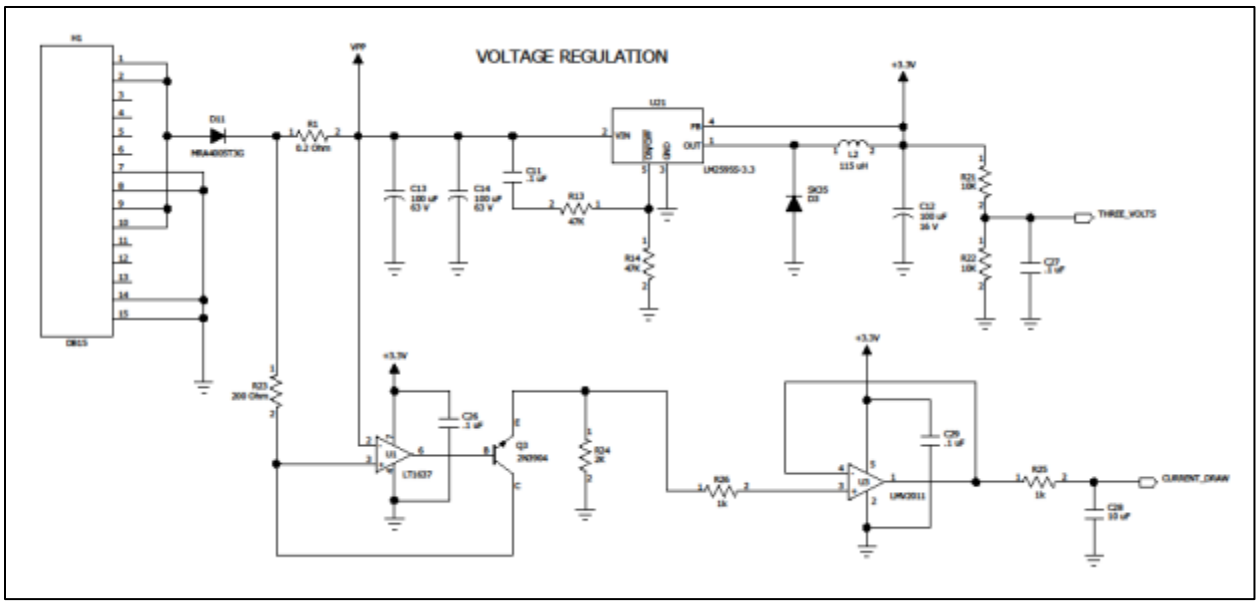

Fig. 10 (e) Voltage regulation circuit

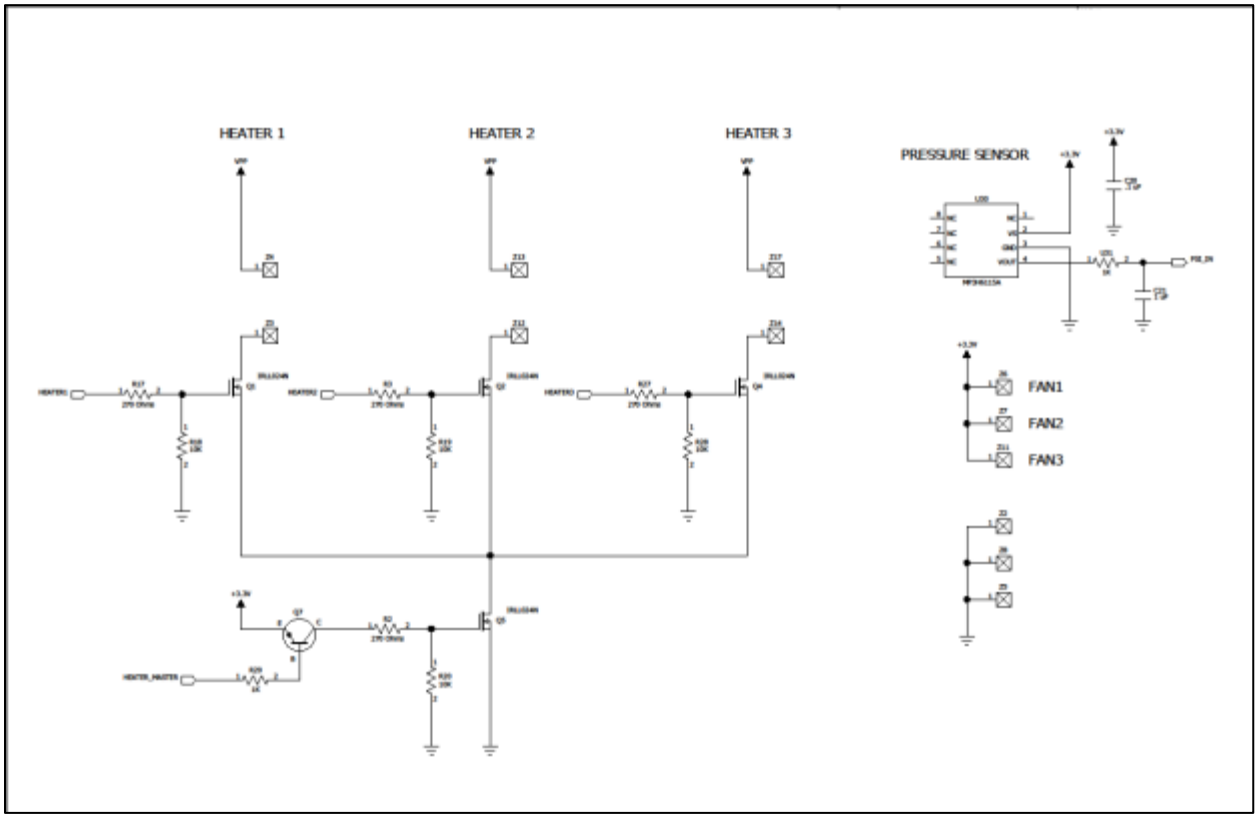

Fig. 10 (f) Circuit for three heaters, three fans and pressure sensor

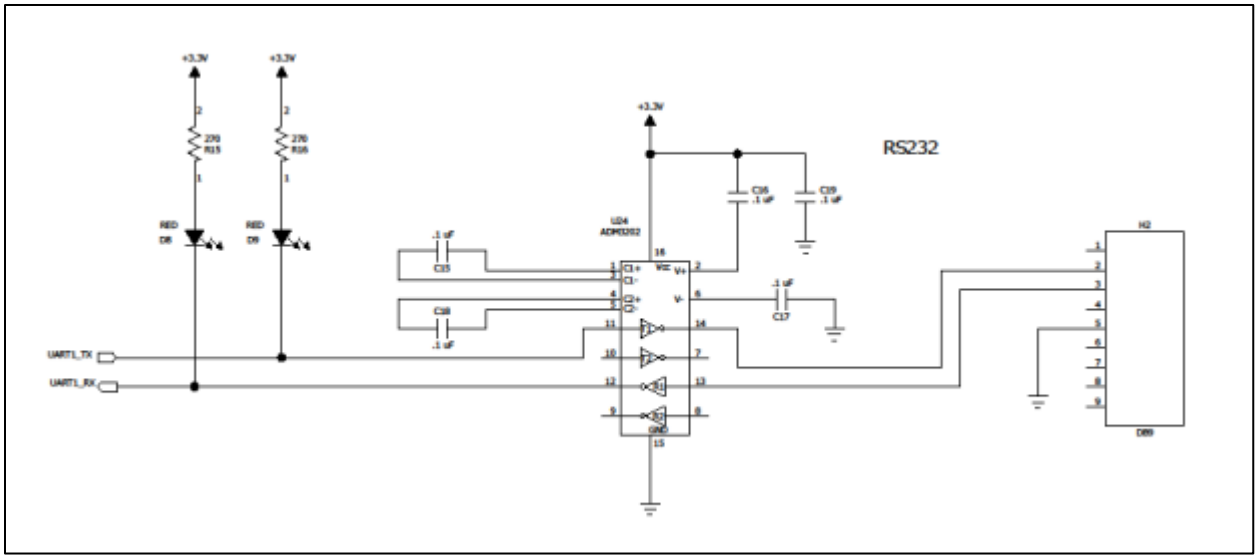

Fig.10 (g) Circuit for RS232

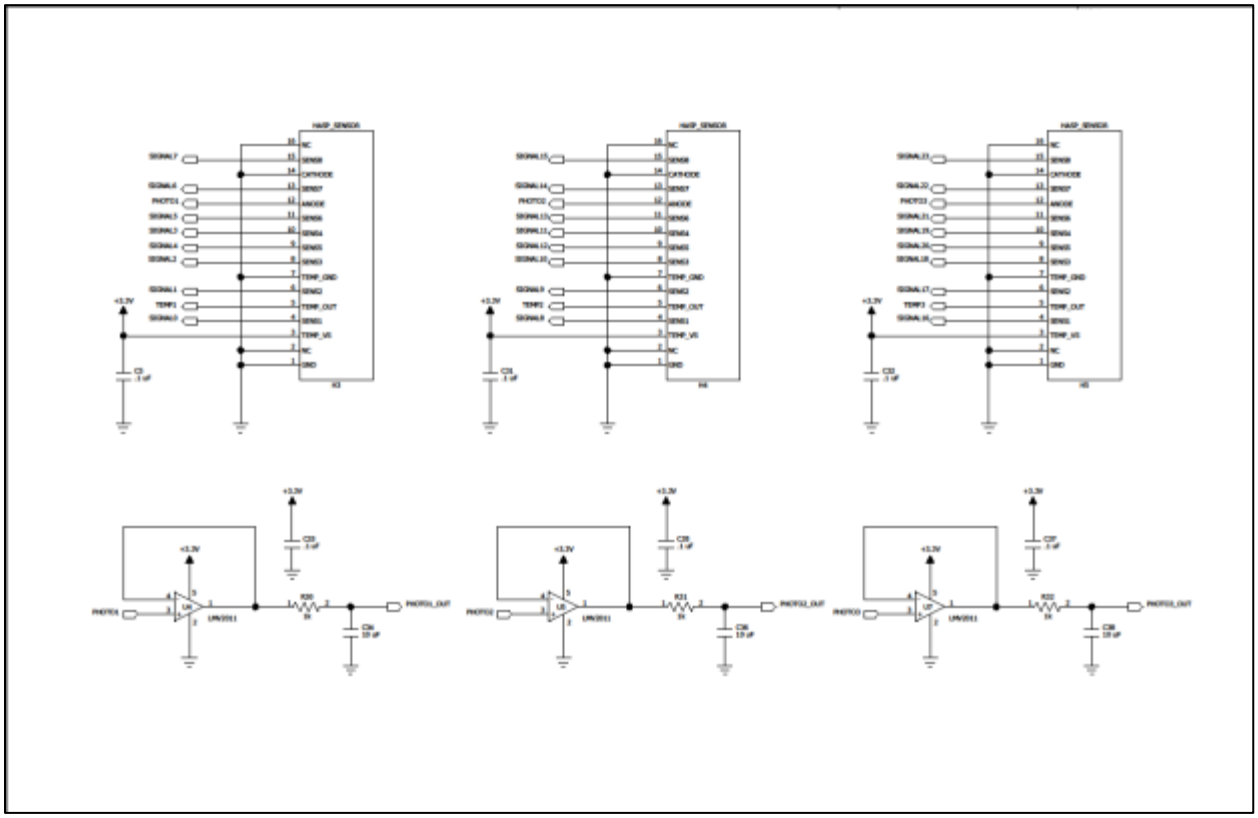

Fig.10 (h) Circuit for three ozone sensors boxes and three photo (light) sensors

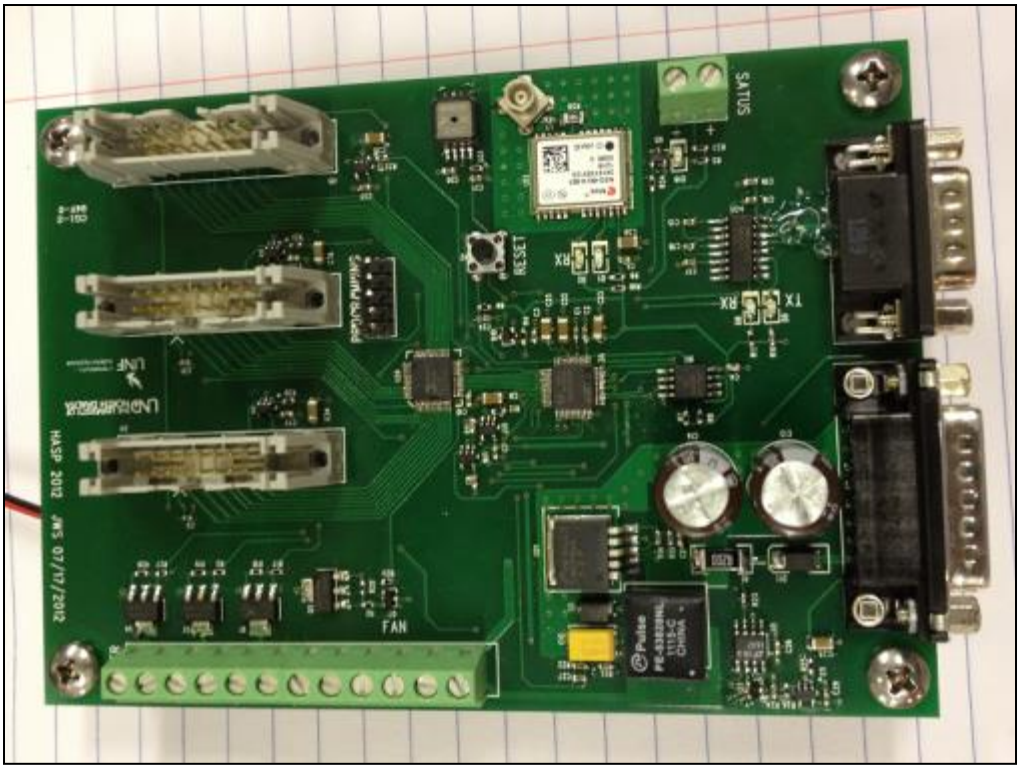

Fig. 10 (i) Picture of microcontroller PCBs

Payload Integration and Thermal Vacuum Test

The payload body, sensors boxes and circuit board were interegrated at the the CSBF, Palestine during July 29 to August 3, 2012. Fig 11(a) to (f) shows pictures of various activites such as integration and testing of payload at CSBF, Palestine, TX.

Fig. 11 (a) Inregration of sensors boxes, payload and PCB, (b) Top view of payload

Fig.11 (c) Doug Granger (HASP) testing the payload, (d) Nirmal testing the Payload

Fig. 11 (e) Ken and Dr. Patel integrating payload on HASP, (f) Dr. Greg Guzik (Director, HASP) testing the payload

The UND-UNF payload was tested in the BEMCO chamber, which is shown in Fig. 11(g and h) for high temperature (+50^{o}C), low temperature (-50 ^{o}C), high pressure (1.5 atm), and low pressure (9 mbar). The measured current draw at 31 VDC is about 40 mA. The payload sucessfuly cleared the thermal vacum test at the CSBF, Palestine, TX on Wednesday, July 31, 2013.

Fig.11 (g) Group of HASP 2013 participants with Dr. Guzik and HASP team at time of the thermal vacumm test and (h) Testing of commonds of payload during the thermal vacuum test chamber by Michael Stewart (HASP) and Jill (CSBF).

Launching of Payload

HASP2013 flight was sucessfully launched from CSBF, Fort Sumner, NM on the first attempt on Monday, Septemeber 2, 2013 (Labor day holiday) morning. Fig. 12 (a) shows the HASP 2013 balloon flight information, while fig. 12 (b) shows preparation of launach at the CSBF, Fort Sumner, NM.

HASP2013 Balloon Flight Information

- **Balloon Manufacturer** Winzen
- **Balloon Type** Zero pressure, 1 cap (W11.82-1E-37 CSBF #979)
- **Balloon Size** 11.82 million cubic feet
- **Parachute Diameter** 79 feet
- **FLIGHT NUMBER: 643N**
- **LAUNCH TIME:09/02/2103 14:57:07 UTC**
- **LAUNCH LOCATION: NASA-Columbia Scientific Balloon Facility**
  Fort Sumner, New Mexico
- **FLOAT START:09/02/2013 16:56 UTC**
- **TERMINATION:09/03/2013 03:25:32 UTC**
- **IMPACT:09/03/2013 04:11:55 UTC**
- **FLOAT TIME:10:29 Hours**
- **IMPACT LOCATION: 33.96 Lat, 112.98 Long, West of Phoenix, AZ**

Fig. 12 (a) HASP 2013 balloon flight information,

Fig. 12 (b) Preparation of launach at the CSBF, Fort Sumner, NM.

Fig. 12 (c) shows the launching of the balloon flight, while the picture of UND-UNF payload during flight in the startosphere is shown in fig. 12(d).

Fig. 12 (c) Launaching HASP2013 balloon flight at the CSBF, Fort Sumner, NM.

(Courtesy: http://laspace.lsu.edu/hasp/images/2013/MIT/images/IMG_1384.JPG and MIT Team)

Fig.12 (d) UND-UNF sensors payload in the starosphere

The HASP 2013 flight was terminated on September 2, 2013 landing a bit west of Phoenix, AZ area. Fig. 13 (a) shows the flight path of the balloon on a Google map.

Fig.13 (a) Flight path of the balloon on a Google map

The balloon flight was terminated near west of Phoenix, AZ. Fig. 13 (b) shows the impact of HASP on the ground after termination, while fig. 13 (c) shows the recovery team member with HASP. The UND-UNF payload was survived from the direct hit on the ground.

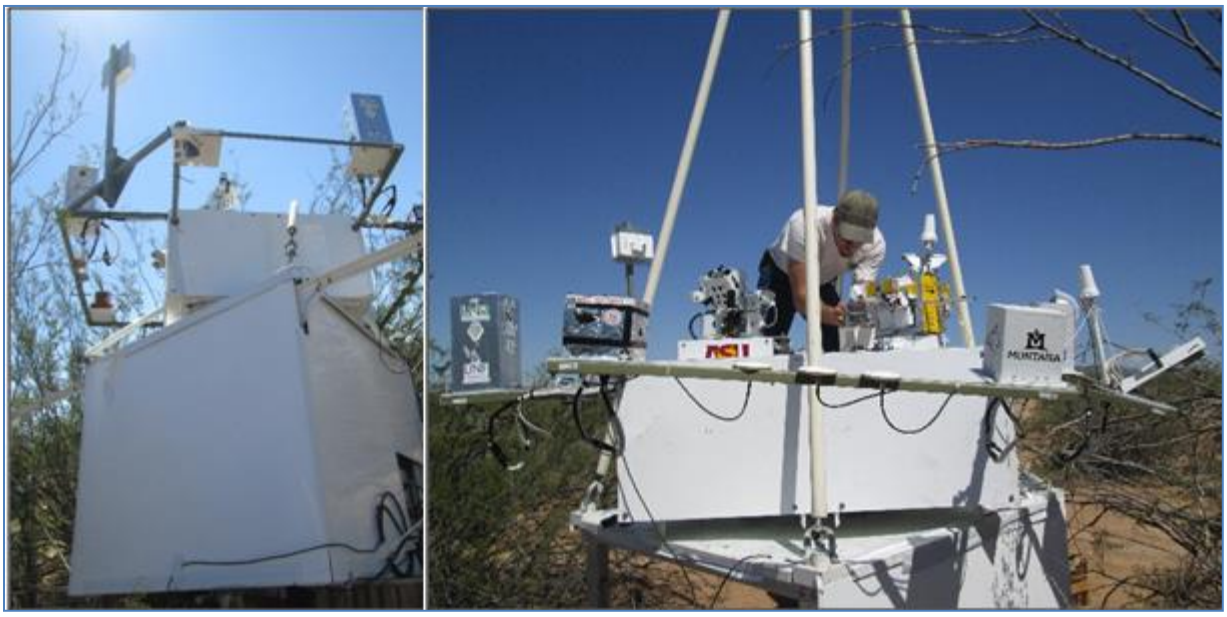

Fig. 13 (b) Impact of HASP on the ground and (b) the recovery team member with HASP.

(Courtesy: http://laspace.lsu.edu/hasp/images/2013/MIT/images/IMG_1493.JPG and MIT Team)

Detection of ozone profile in the Starosphere

Fig. 14 shows various steps for the detection of oozne by the sensors payload during the flight.

How Ozone was detected?

- Change in concentration of ozone with altitude
- Detection of ozone gas by three sensors boxes mounted on the three side of payload in terms of change in electrical resistance of sensors
- Change in resistance was converted into change in analog voltage by electronic circuits-multiplexer, amplifier and bridge circuit
- Analog voltage was converted into digital by A/D converter and microcontroller circuit
- Signal communication made by serial data RS232 + microcontroller
- Data were transferred from payload to HASP Platform computer by RS232
- Data were transferred from HASP Platform computer to HASP Ground computer by telemetry
- Data files were uploaded on HASP website
- Download data files into the user laptop from HASP website as RAW files
- Converted RAW files directly into EXCEL files using c programming and developed software.
- EXCEL sheet was made for sensors voltage data, convert into resistance data. Added temperature, photo voltage and altitude information. Converted resistance values into concentration of ozone gas using the trend line equations of the calibration plots.
- Made the profile plots for the altitude versus measured concentration of ozone and compared measured profile with the theoretical plot profile.

Fig.14 Steps for the detection of ozone by the payload

During the flight, UND-UNF sensors payload measured the ozone profile. The payload sent data files of 2KB every 9 to 10 minutes during the flight time through the NASA-HASP computer and was uploaded on the HASP website. We downloaded all the RAW data files, and converted RAW files into one EXCEL file using the software program. It was found that the sensors,

hardware and software worked very smoothly. There was no need to upload the special commands to reboot the payload system during the flight. Two minor issues were observed, which were (i) GPS failed after 60000 feet and (ii) mixing of data stream with other payload.

Results and discussion:

Fig. 15 (a) shows the HASP 2013 balloon flight profile. The altitude profile was measured by the initially by UND-UNF payload GPS and then HASP GPS. This flight profile has few times missing data due to switch over of our GPS to HASP GPS during ascending as well as no power and / or communication during termination and impact. We are trying to borrow the flight profile from other groups for comparison and verification purpose.

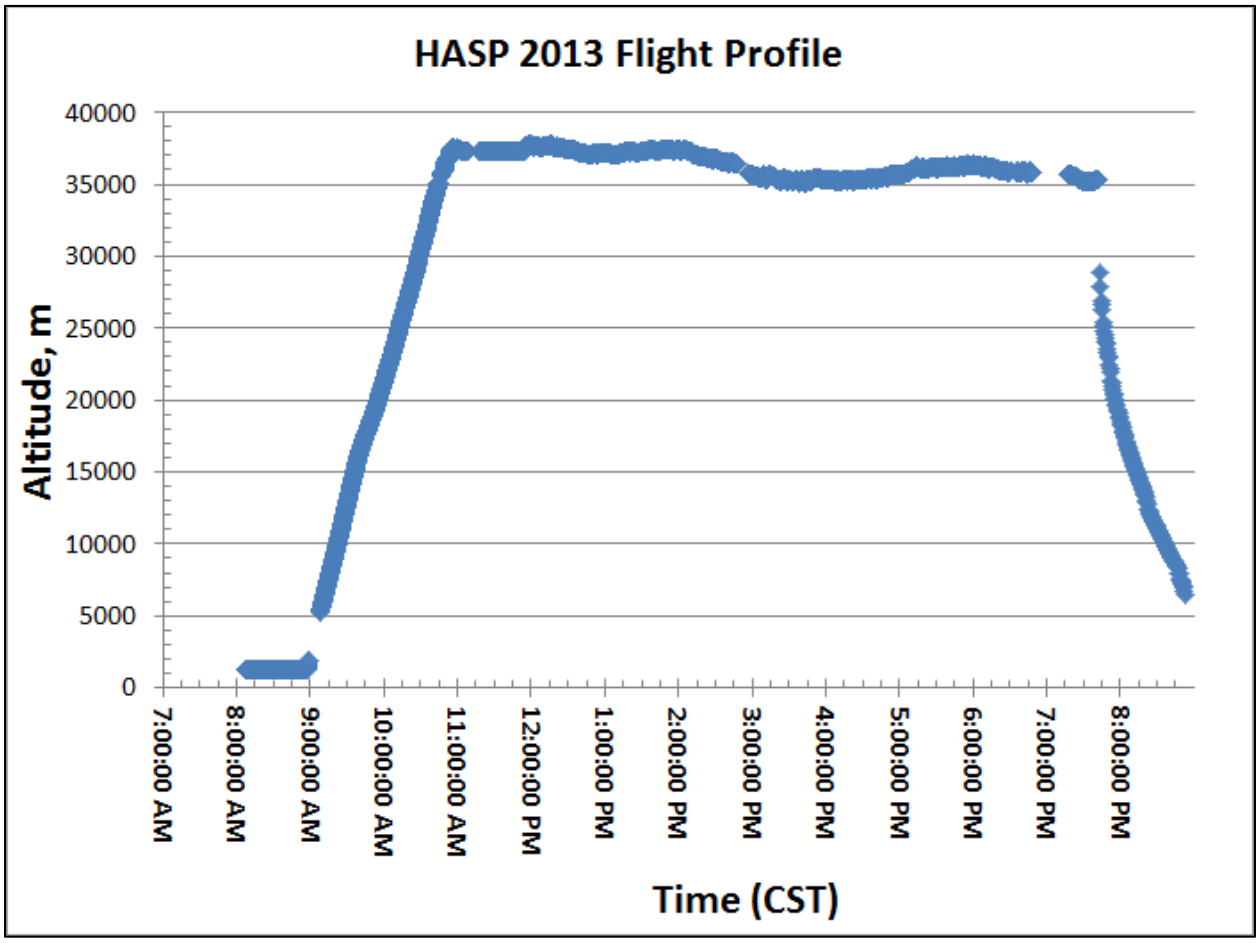

Fig.15 (a) HASP2013 flight profile

Fig.15 (b) shows the variation of pressure with the altitude during the flight. Pressure was measured by a pressure sensor mounted on the PCB of the payload. It was found that the pressure was decreased with increase of the altitude up about 16 km and then nearly saturate with increase of altitude up to the float. The saturation of pressure around 100 mbar was due to the technical limitation of our pressure sensor. We are going to replace this pressure sensor with one having lower mbar range in the next balloon flight.

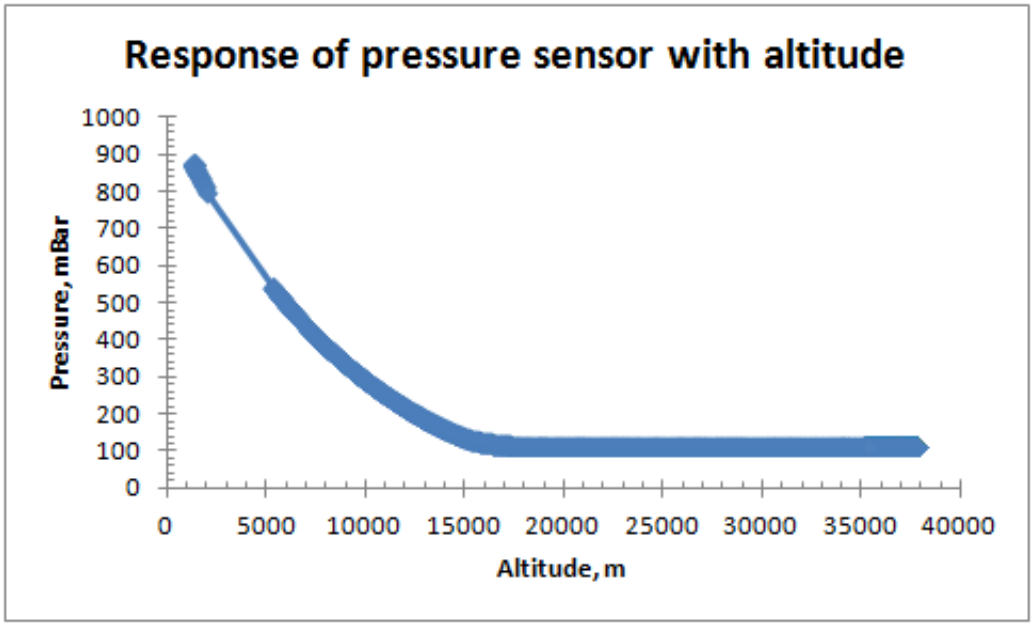

Fig.15 (b) Variation of pressure with altitude

Power budget during flight

Fig. 16(a) shows the voltage applied to the payload during the flight. It was found that applied voltage remain nearly constant about 3300mV. The current drawn by the payload during the flight is shown in fig. 16(b). Payload draw minimum 30 to 40 mA when all three heaters were off, while maximum about 380 mA when all three heaters were on. The power budget was maintained under the upper limit of HASP requirement during the flight.

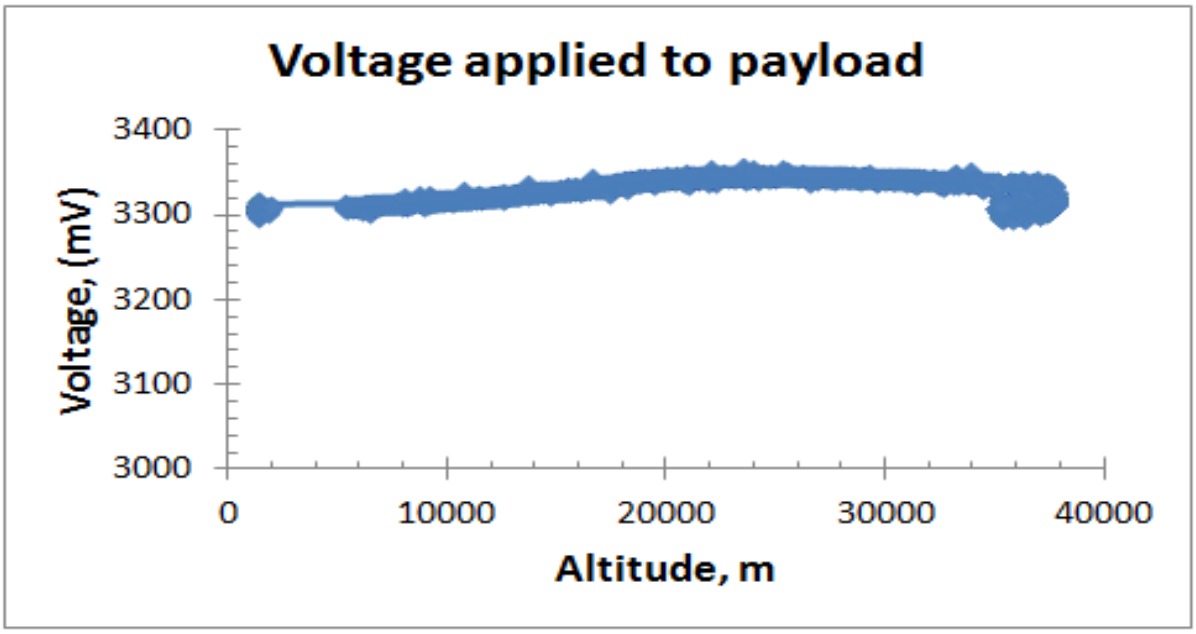

Fig.16 (a) Voltage applied to the payload during the flight.

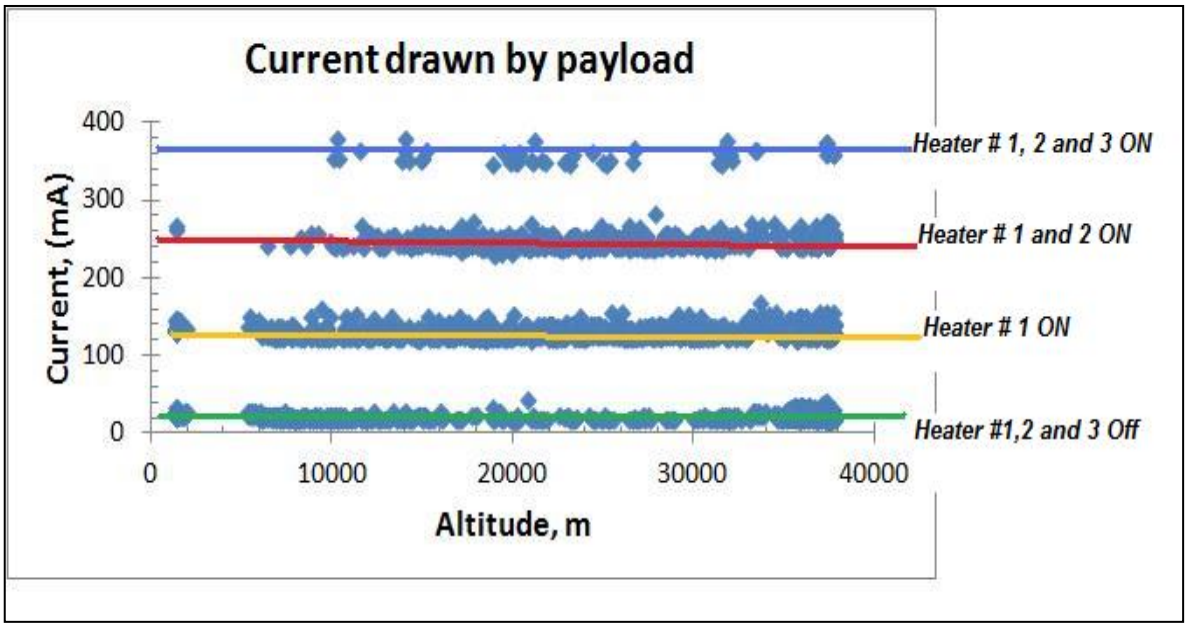

Fig.16 (b) Current drawn by the payload during the flight

Thermal stability of payload

The variation of temperature of ozone sensors box #1, 3 and 4 with altitude during the flight is shown in fig.17 (a), (b) and (c), respectively. The temperature of sensors was controlled in the range of 300 ± 6 K using an On-Off controller, a polyimide flexible heater (MINCO make) and a temperature sensor TMP 36). Temperature of sensors was well controlled during the most of time of the flight. Some of data were missing due to the issue of mixing data. Table-1 shows the measured average temperature, standard deviation and one sigma standard error of temperature of sensor box#1, box#3 and box#4.

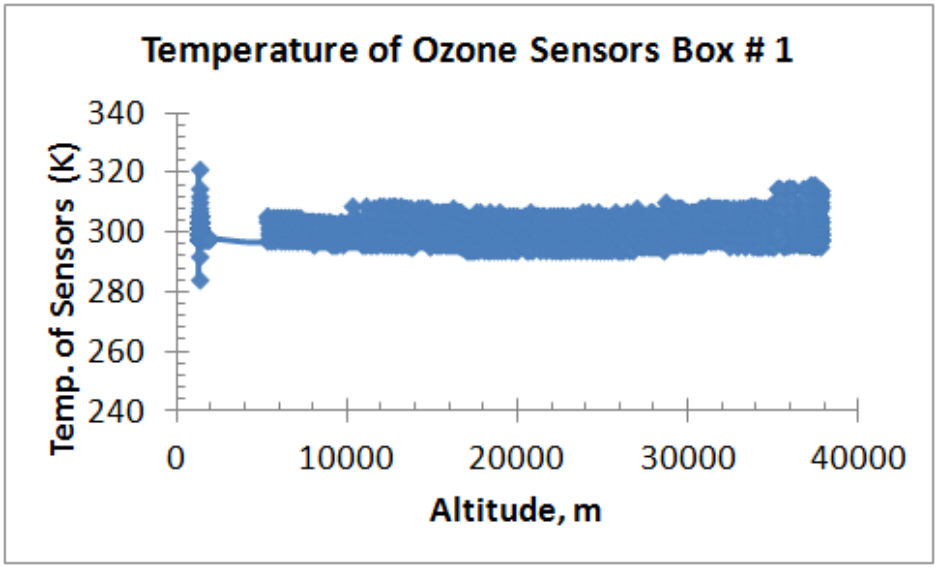

Fig.17 (a) Temperature of ozone sensors box#1

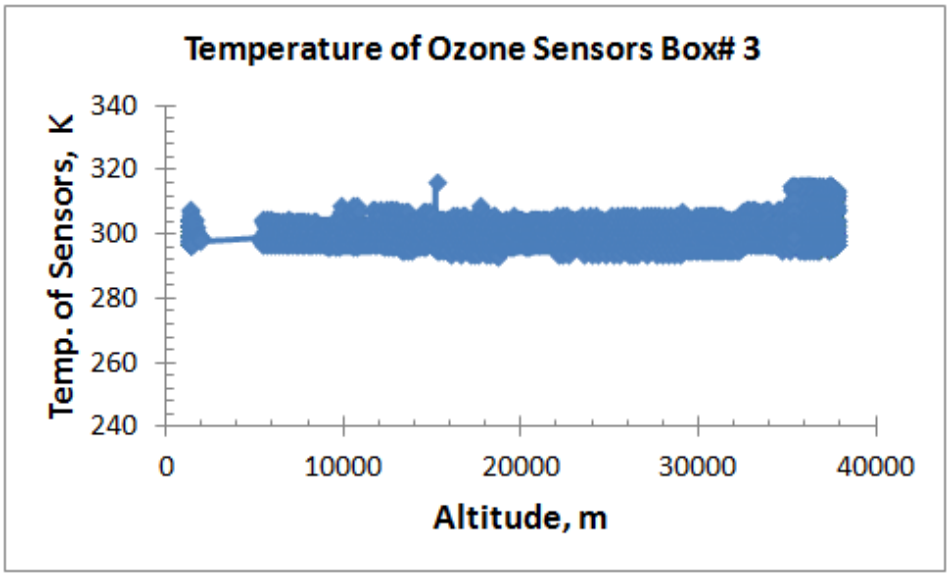

Fig.17 (b) Temperature of ozone sensors box#3

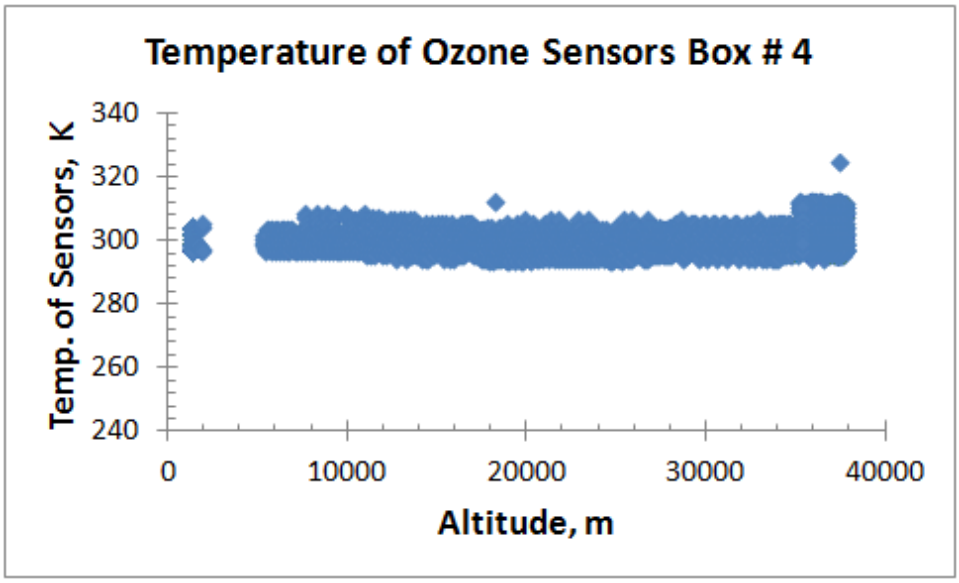

Fig.17 (c) Temperature of ozone sensors box#4

Sensors Box #	1	3	4
Average temp (K)	300.6	300.5	300.6
Standard deviation (K)	5.5	5.6	6.0
standard error	0.1	0.1	0.1

Table1. Average temperature and standard deviation of temperature of sensors array 1, 3 and 4 during the flight.

The variation of photo voltage generated by the photo diodes mounted on sensor box #1, 3 and 4 during the flight is shown in fig 18 (a), (b) and (c), respectively. It was observed that measured photo voltage was larger in the altitude range about 14000 to 28000 m. The larger photo voltage confirmed the presence of ultra violet Sun light. In the presence of that UV light oxygen converted into ozone gas.

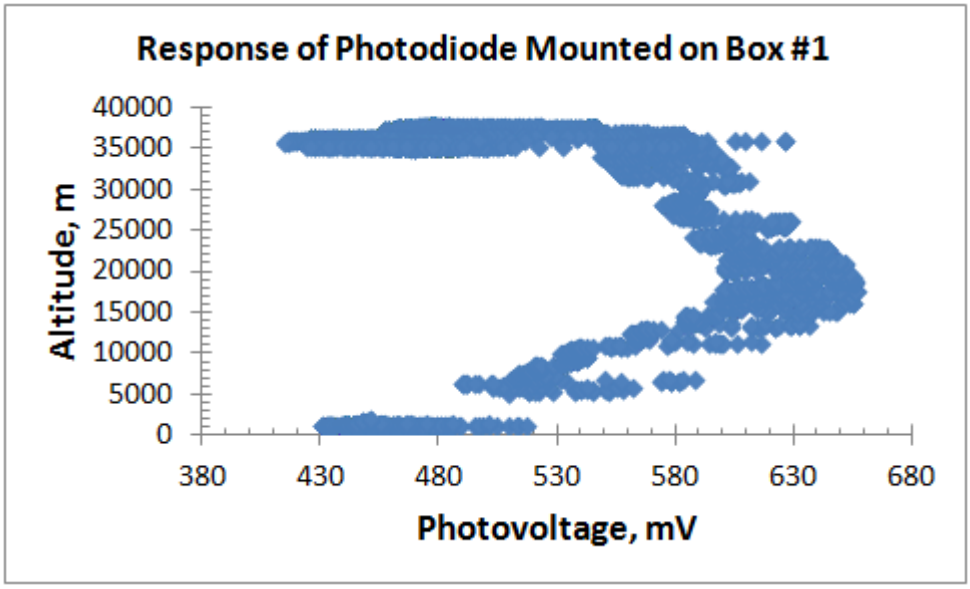

Fig.18 (a) Variation of photo voltage on sensor box#1

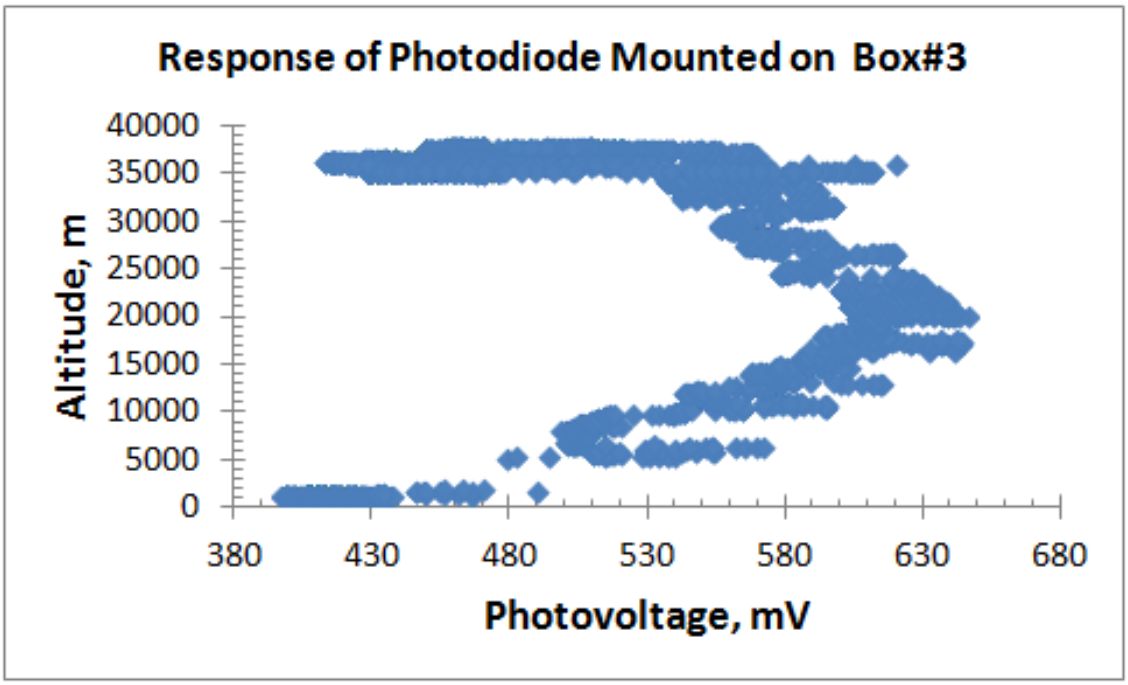

Fig.18 (b) Variation of photo voltage on sensor box#3

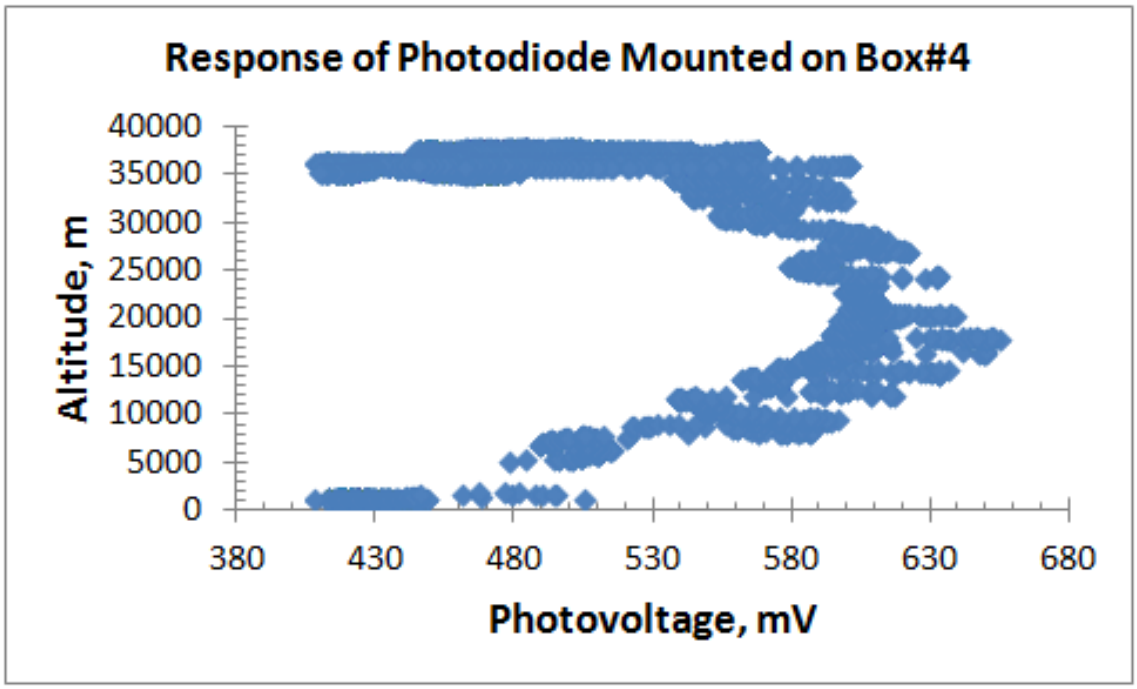

Fig.18 (c) Variation of photo voltage on sensor box#4

Discussion of Measured Data

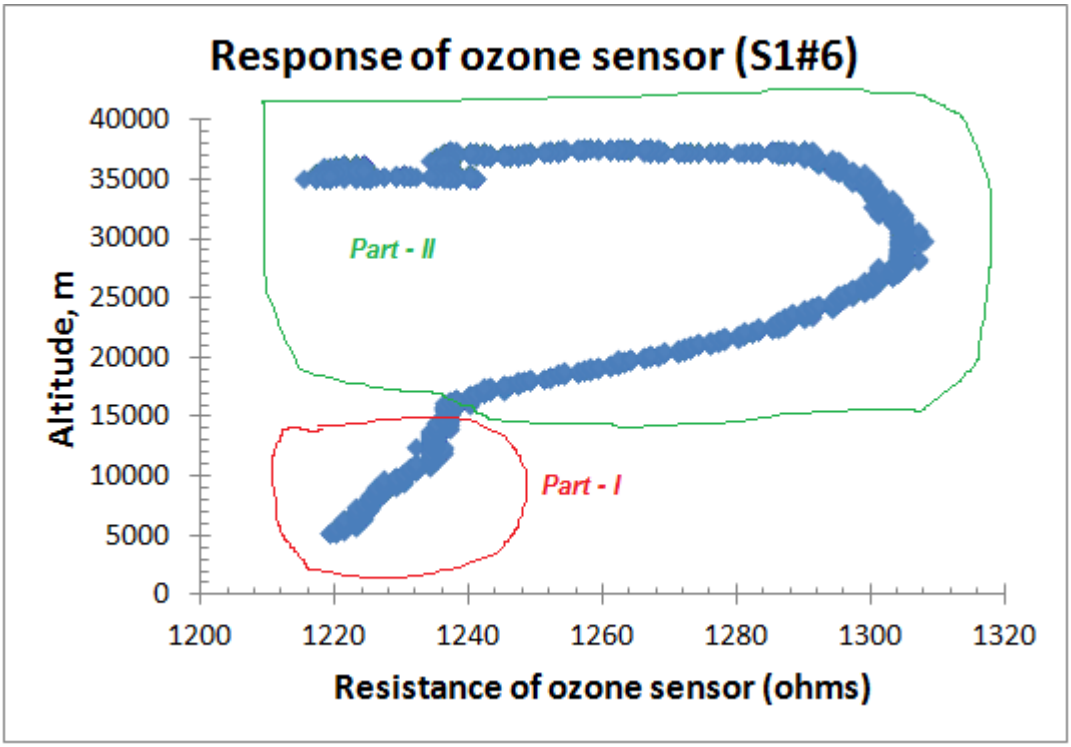

Fig.19 (a) Response of ozone sensor of **Box#1** (S1#6) with complete range of altitude

Sensor S1#6 was randomly picked for the discussion of response of sensor with the entire range of altitude of balloon. Sensors of Box-1 were made of improved version of nanocrystalline ITO thin films compare to our previous balloon flights. These sensors have better selectivity and sensitivity with ozone gas. Fig.19 (a) shows how the variation of resistance of sensor with the altitude of balloon. Both plots of fig.19 (a) can be divided into two parts.

(i) Part-I is circled by the red color. This part-1 has altitude from ground level to about 12000 meter. This part-1 covers atmosphere and troposphere. The resistance of sensor was affected by due to interaction of the sensor surface with the most of reducing gases presence in the atmosphere and troposphere. Note that there was no effect of cold temperature on sensor because the temperature of gas sensors was controlled and maintained to about 293 to 308 K. The amount of anthropogenic ozone in this zone is very low compared to that of available pollutant gases and smog, which was not measured correctly due to interference of the large amount of reducing gases and smog. In addition, amount of available UV light is less to convert oxygen into ozone.

(ii) Part-II is circled by the green. The resistance of ozone sensor was increased from altitude 12000 meter to about 28000 meters and then slowly to decrease up to

maximum altitude at the float. This region is known as the stratosphere (Refer Fig.1 (b). We are interested to measure the ozone profile mainly in this region. The concentration of ozone is higher in the middle of stratosphere in the presence of ultra violet rays from the sunlight. Ozone is oxidizing gas and its concentration depends on amount of available ultra violet Sun light. Upon adsorption of charge accepting molecules at the vacancy sites from ozone oxidizing gas, the electrons are effectively depleted from the conduction band of n-type Indium tin oxide (ITO) semiconductor sensor. Thus, this leads to an increase in the electrical resistance of n-type ITO gas sensor. At the maximum float of balloon, the concentration of ozone should change with time due to mixing ratio and availability of ultra violet rays from the sunlight.

We observed similar observations in all the sensors (S1#1 to S1#8) of box-1. Response of sensors of box-3 was also similar to box-1. Response of sensor #S3-2 of box-3 is shown in Fig.19 (b). Sensors of Box-3 were made of nanocomposite of ZnO + ITO thin films. Both sensors boxes #1 and 3 have good selectivity of ozone gas in the stratosphere (part-II) compare to that other pollutant gases in the atmosphere and troposphere (part-I).

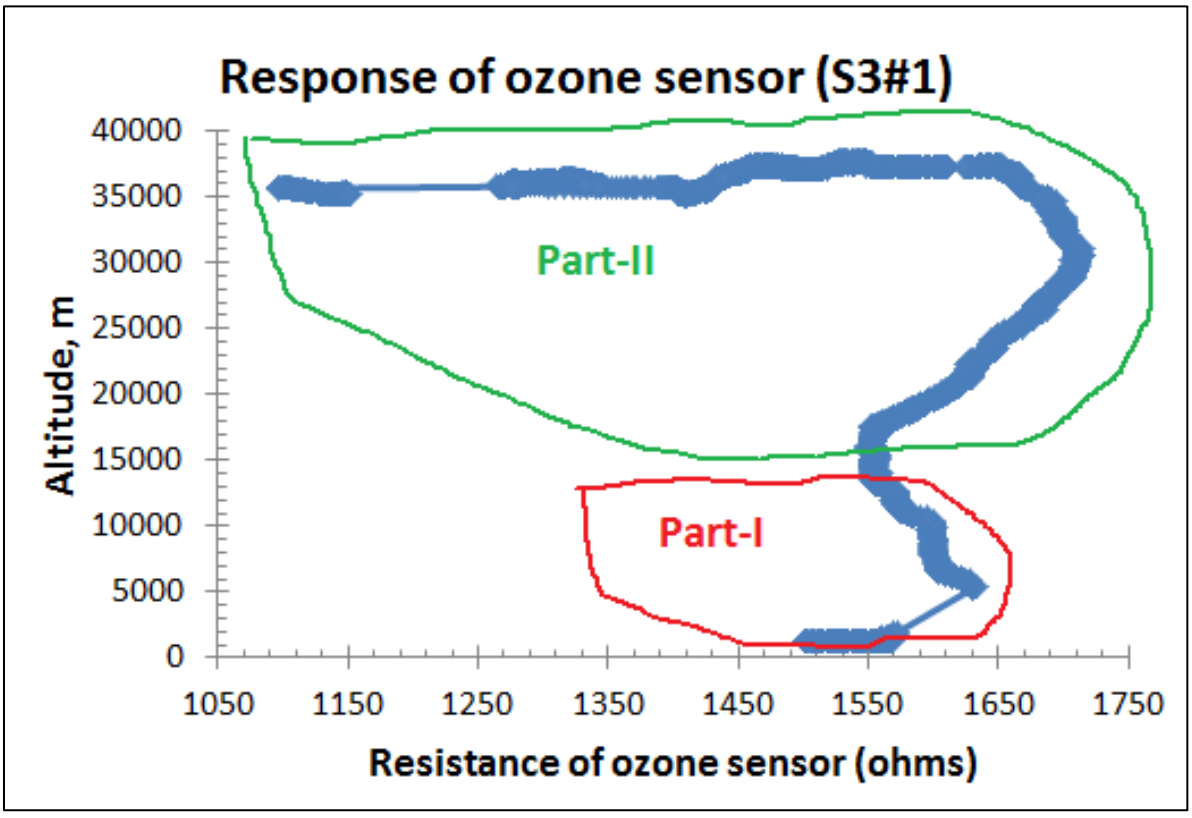

Fig.19 (b) Response of ozone sensor of **Box# 3** (sensor S3#1) with entire range of altitude

Response of one of sensors of box #4 with the entire range of altitude of balloon is shown in the 19 (c). Sensors of box-4 were made of nanocomposite of WO_3 + ITO thin films. We have

observed earlier that WO_3 + ITO thin films sensors of box#4 have good selectivity as well as sensitivity with the reducing gases than that of oxidizing gases. We have used these sensors purposefully to explore measurements of some gases in troposphere and atmosphere and also to compare its response in stratosphere. It is observed that the peak in Part-I (circled by red color) is larger than the peak in Part-II (circled by green color) in fig.19 (c). The change in resistance of sensor during journey from ground to altitude about 15000 mm is larger, while the change in resistance of sensor is very small in the stratosphere. Even though sensor responded with interference gases, sensor was able to detect ozone in stratosphere with less sensitivity. We observed similar observations in all the sensors (S4#1 to S4#8) of box-4. Thus it was concluded that sensors boxes #4 have poor selectivity of ozone gas in the stratosphere (part-II) compared to that other pollutant gases in the atmosphere and troposphere (part-I***).***

We therefore have not presented the calibration of plots of the box#4 in this report.

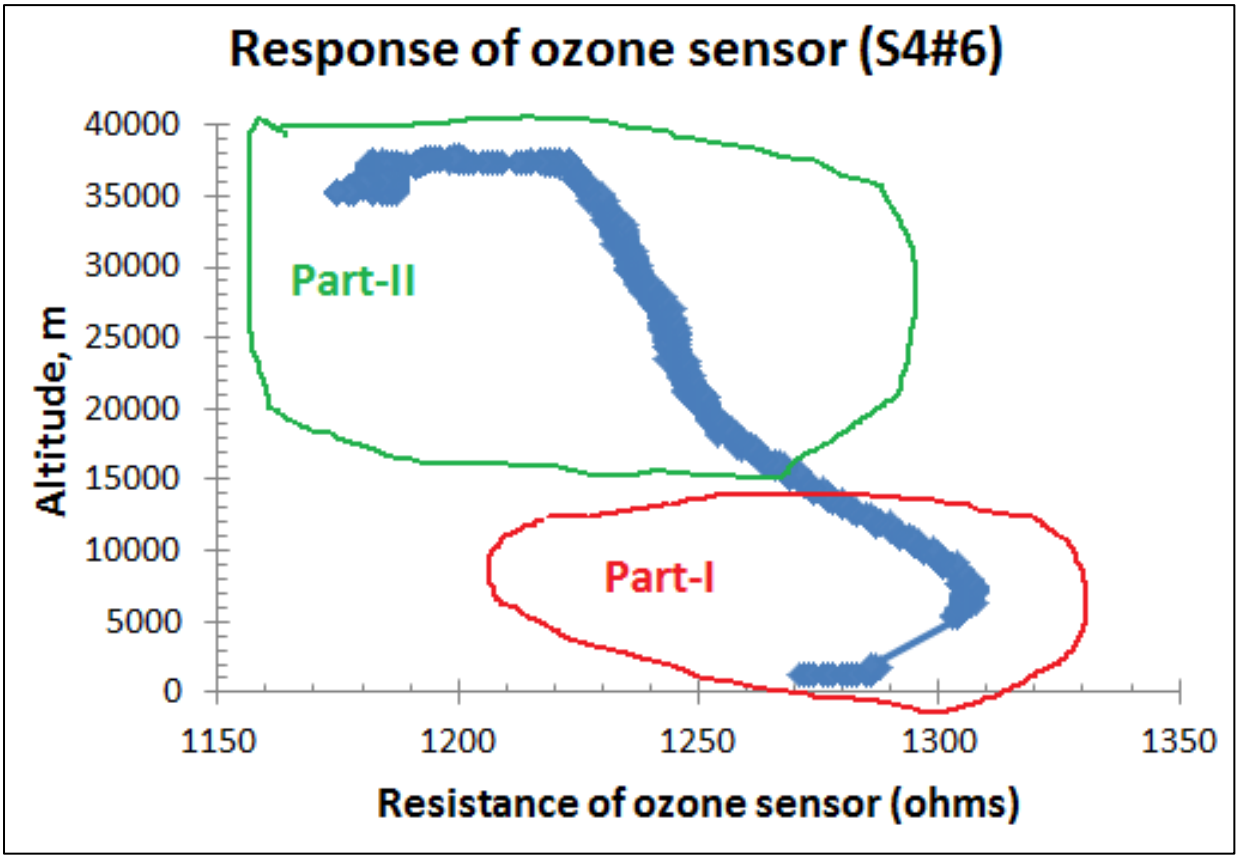

Fig.19 (c) Response of ozone sensor of **Box#4** (sensor S4#6) with complete range of altitude

Response of sensors during the float

(i) Just before float

Variation of ozone concentration with time just before float is shown in fig.19 (e). The plot looks like the damping of oscillations. This is due to the fact that the balloon slow down after ascend journey and then nearly stabilize in the float. The measured concentration of ozone by sensor was continuously decreased from the maximum concentration of ozone during these time period, which is shown in fig. 19 (e).

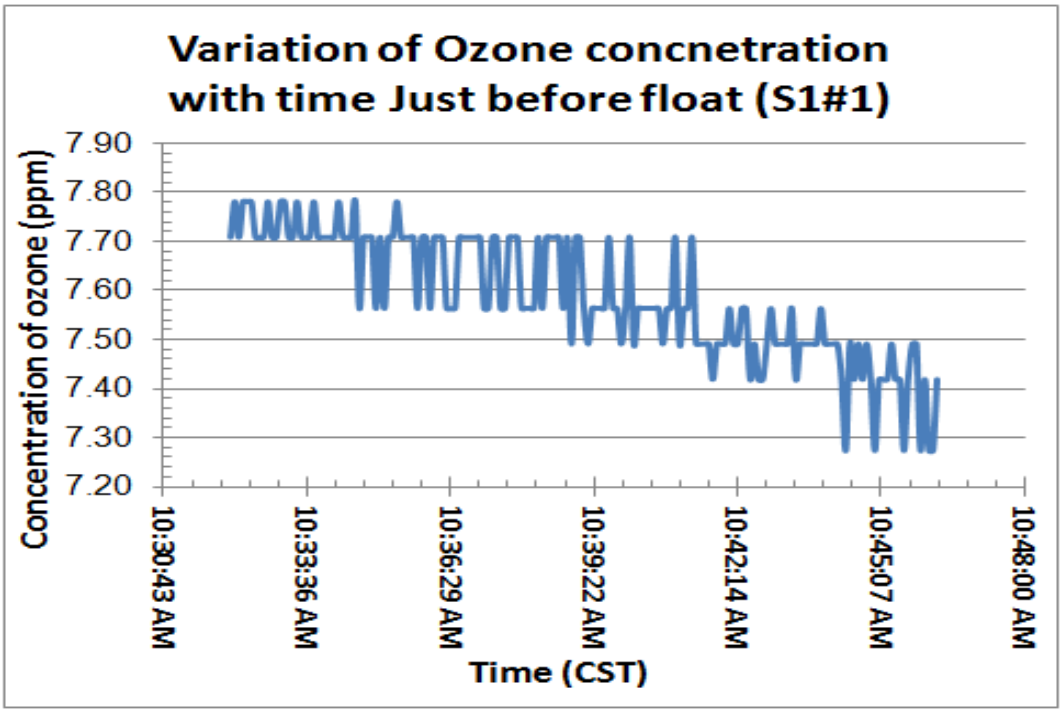

Fig.19 (e) Variation of concentration of ozone just before float with time

(ii) During float

Variation of ozone concentration with time (AM) during float is shown in fig.19 (f). The measured concentration of ozone by sensor was slowly decreased with time during these time period, which is shown in fig. 19 (f). The slow decrease in ozone may be due to the fact that the decreasing of amount of UV light near sensor to convert oxygen into ozone and mixing ratio.

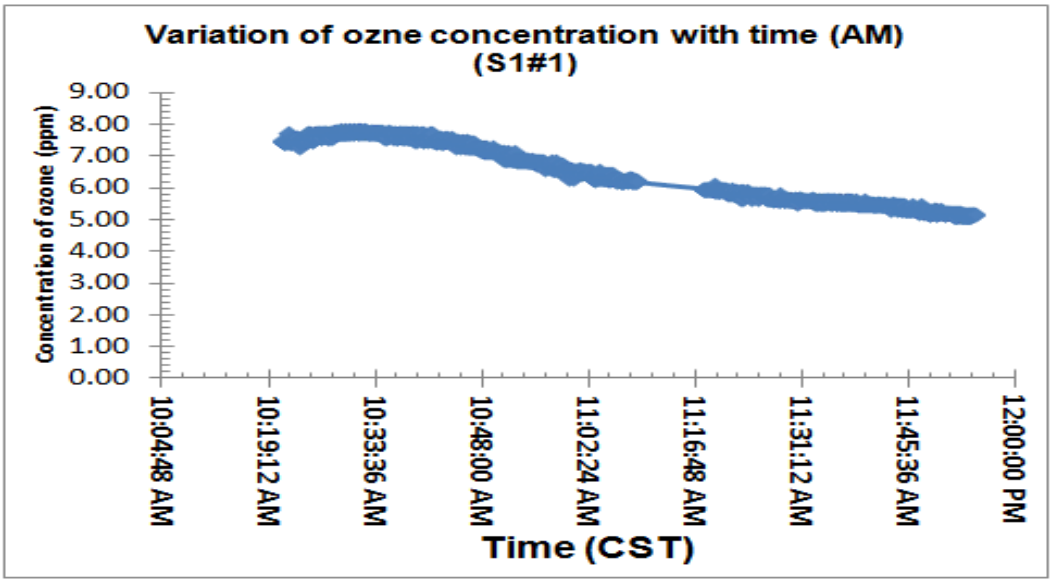

Fig.19 (f) Variation of altitude of balloon during float with time

Variation of ozone concentration with time (PM) during float is shown in fig.19 (g). The measured concentration of ozone by sensor was decreased with time during these time period in stepwise, which is shown in fig. 19 (g). The decrease in ozone may be due to the fact that the decreasing of amount of UV light near sensor to convert oxygen into ozone.

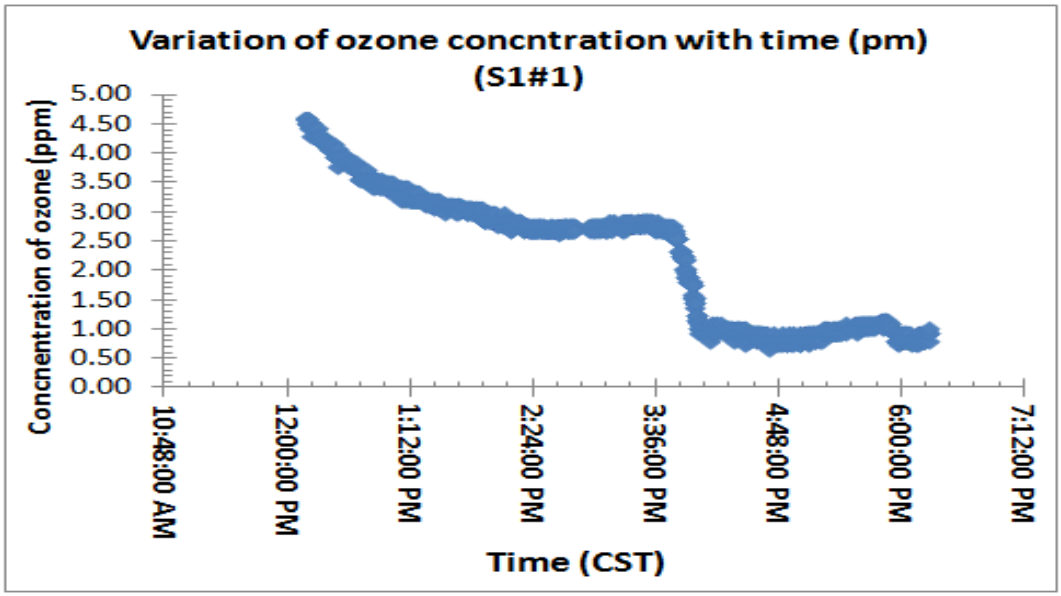

Fig.19 (g) Variation of concentration of ozone during float with time

Response of sensors box #1, 3 and 4 with the altitude is shown in fig.20 (a) to (v). Some part of Part-I of Fig 19 (a) to (c) was excluded in these plots. We focused mainly the stratosphere range to measure the ozone profile.

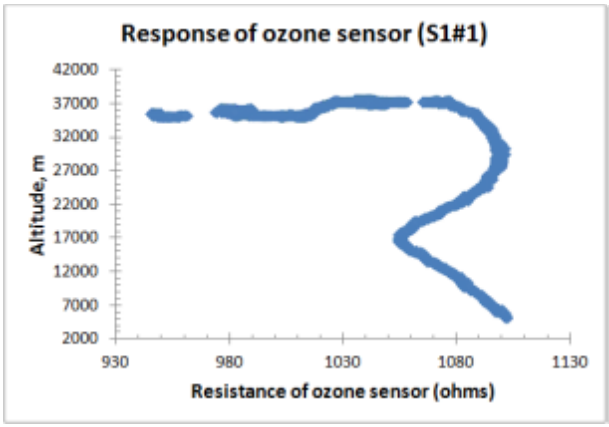

Fig.20 (a) Response of ozone sensor (S1#1)

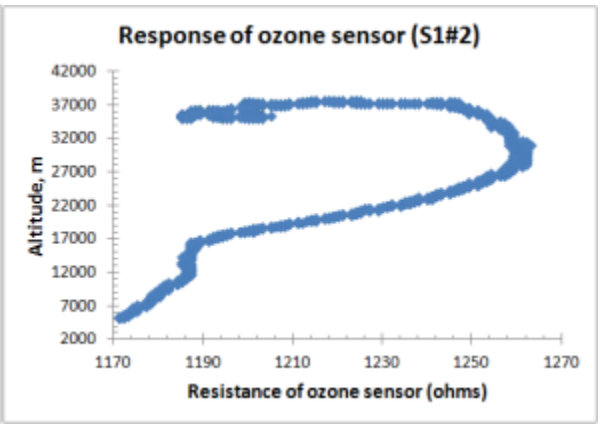

Fig.20 (b) Response of ozone sensor (S1#2)

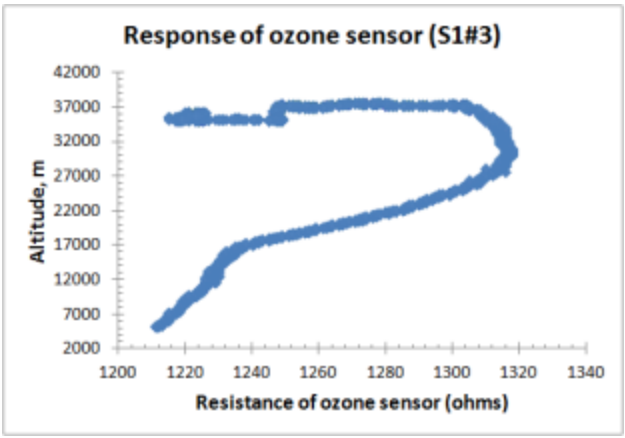

Fig.20 (c) Response of ozone sensor (S1#3)

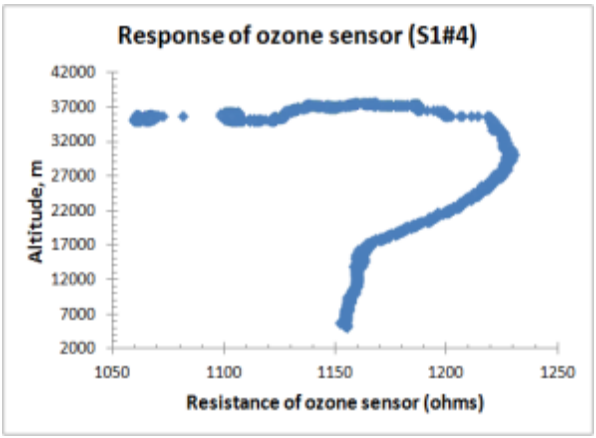

Fig.20 (d) Response of ozone sensor (S1#4)

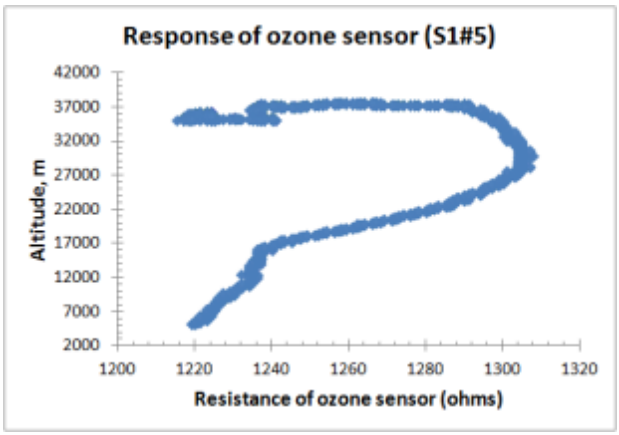

Fig.20 (e) Response of ozone sensor (S1#5)

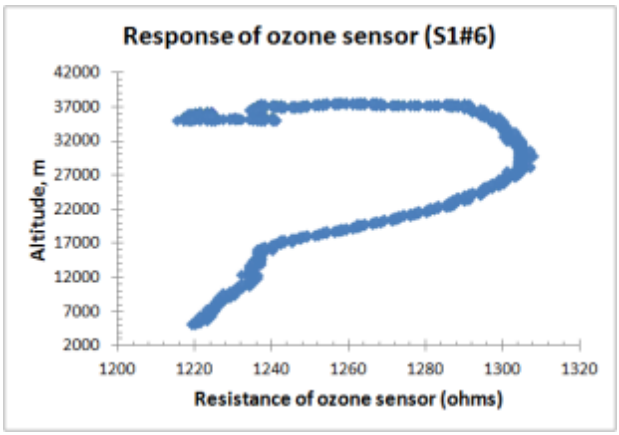

Fig.20 (f) Response of ozone sensor (S1#6)

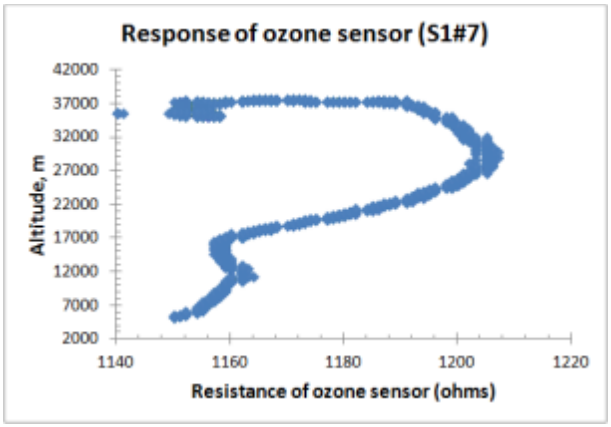

Fig.20 (g) Response of ozone sensor (S1#7)

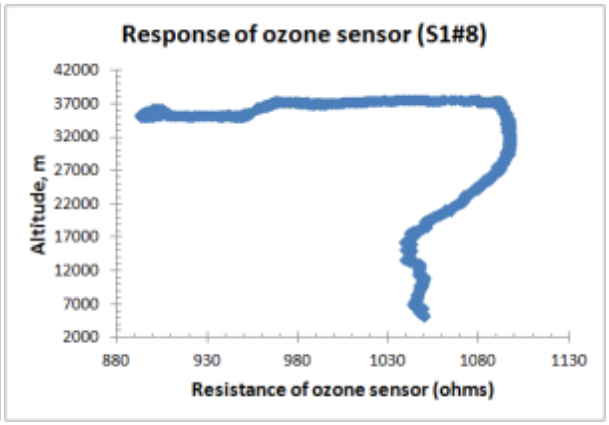

Fig.20 (h) Response of ozone sensor (S1#8)

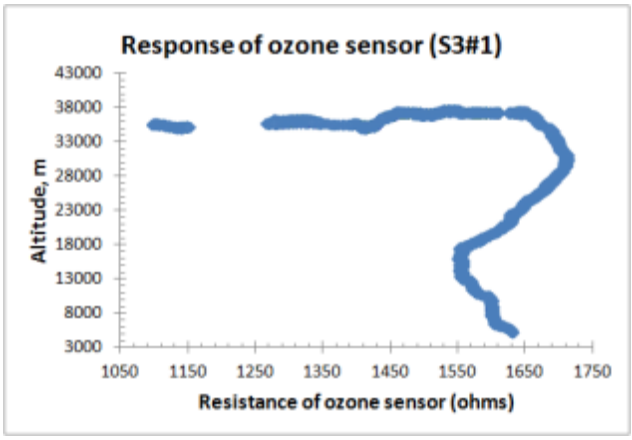

Fig.20 (i) Response of ozone sensor (S3#1)

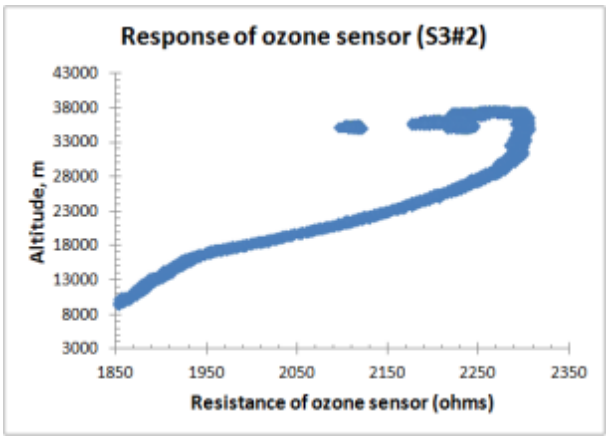

Fig.20 (j) Response of ozone sensor (S3#2)

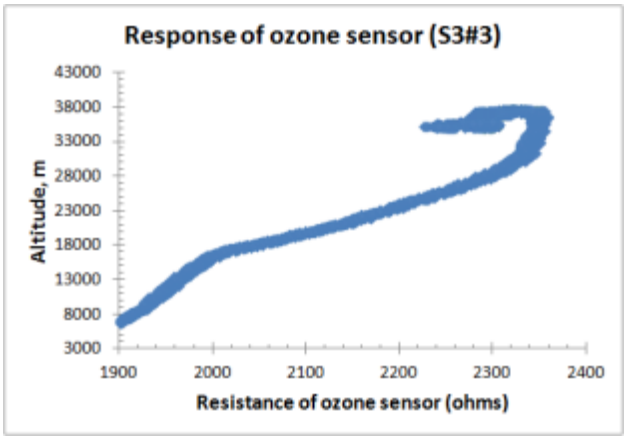

Fig.20 (k) Response of ozone sensor (S3#3)

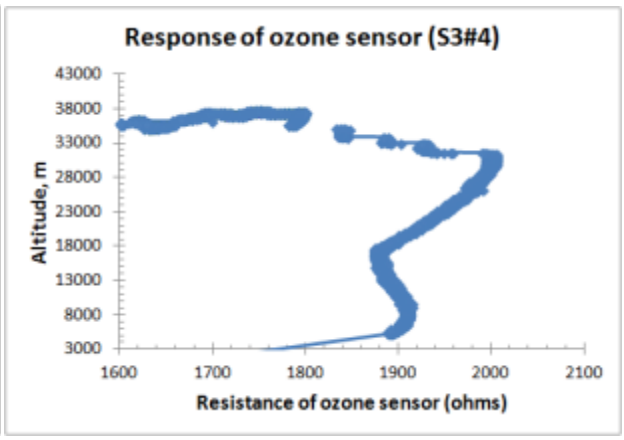

Fig.20 (l) Response of ozone sensor (S3#4)

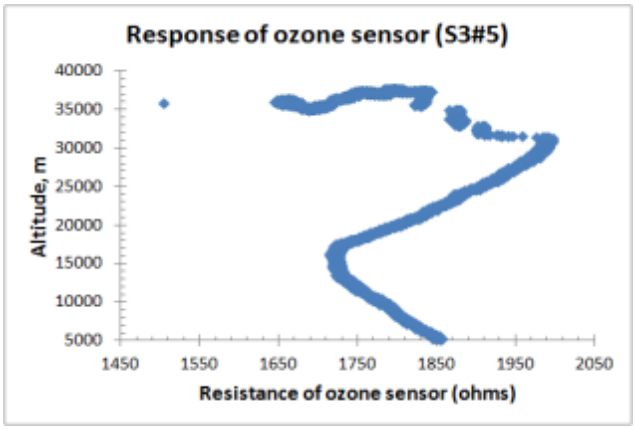

Fig.20 (m) Response of ozone sensor (S3#5)

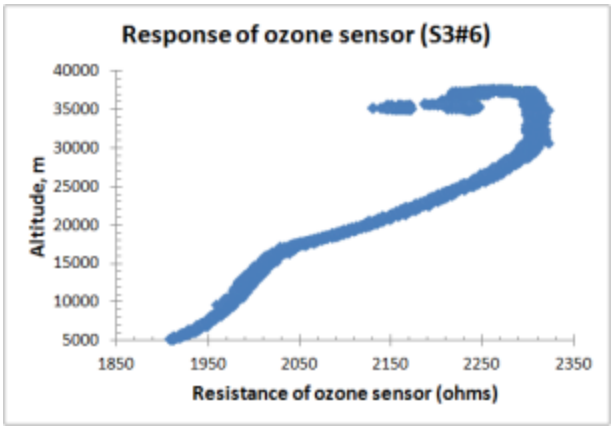

Fig.20 (n) Response of ozone sensor (S3#6)

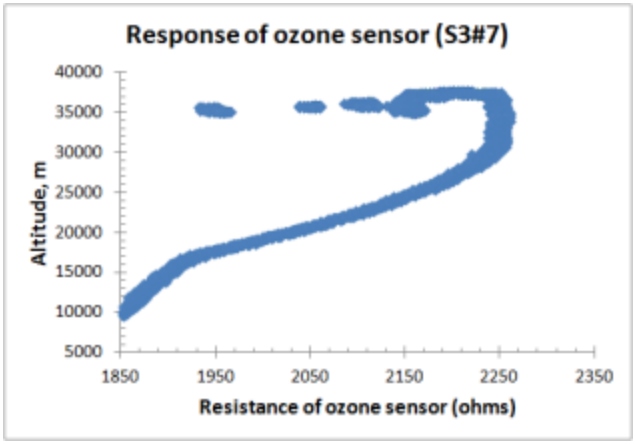

Fig.20 (o) Response of ozone sensor (S3#7)

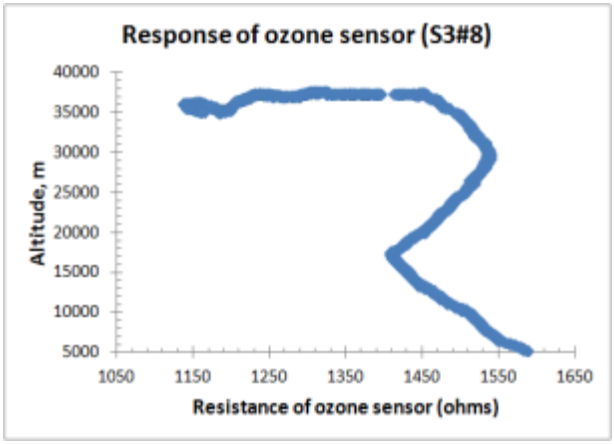

Fig.20 (p) Response of ozone sensor (S3#8)

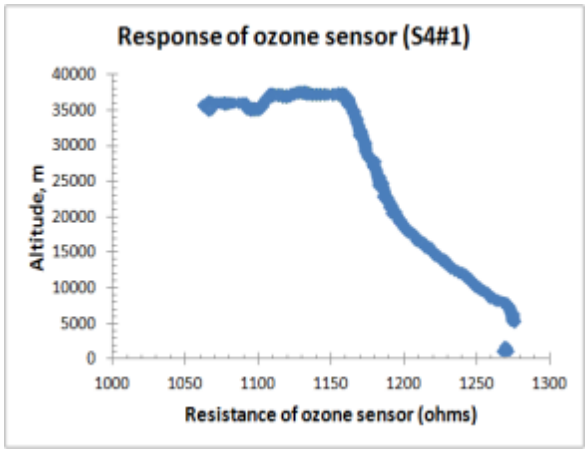

Fig.20 (o) Response of ozone sensor (S4#1)

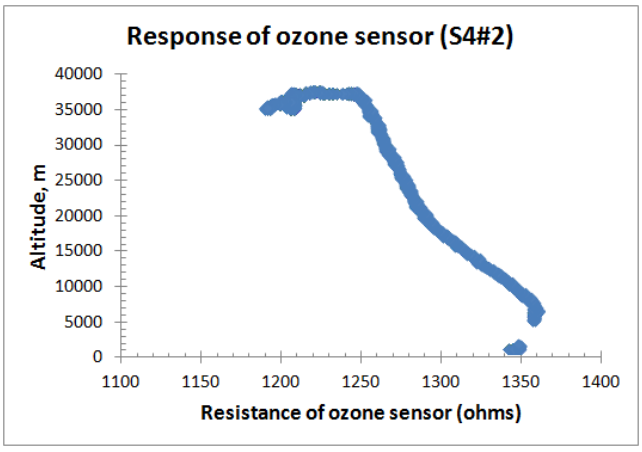

Fig.20 (q) Response of ozone sensor (S4#2)

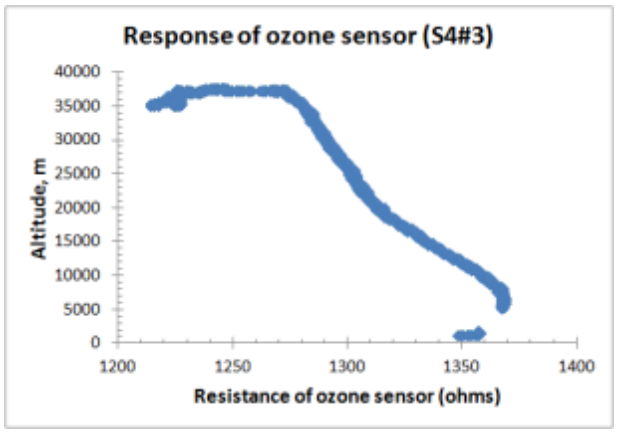

Fig.20 (u) Response of ozone sensor (S4#3)

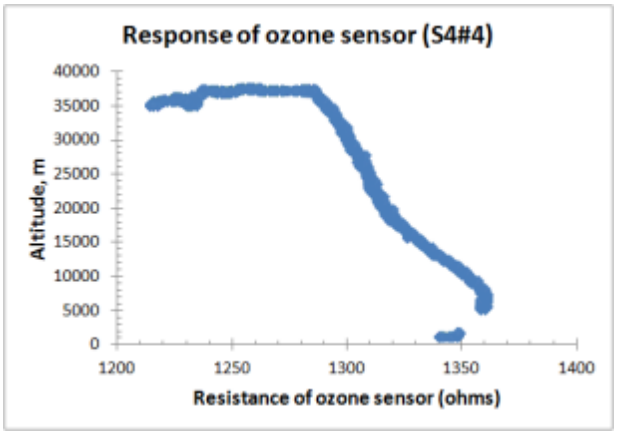

Fig.20 (v) Response of ozone sensor (S4#4)

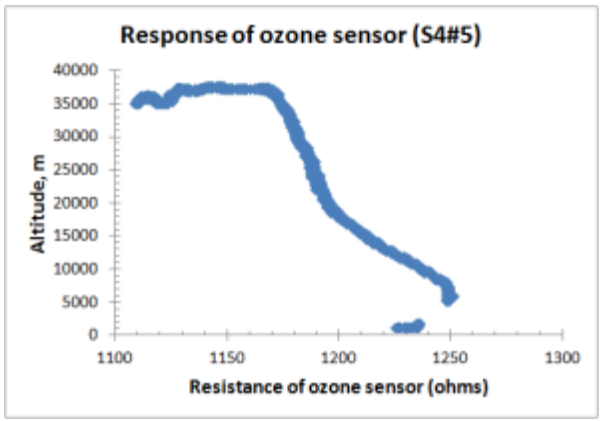

Fig.20 (w) Response of ozone sensor (S4#5)

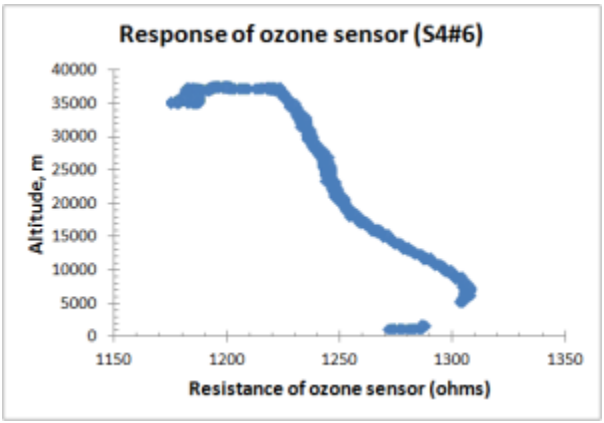

Fig.20 (x) Response of ozone sensor (S4#6)

Fig. 20 (o) to (x) Response of sensors box #4 having sensors S4#1 to S4#6 with the altitude

Using calibration plots shown in fig. 7(a) to (p), the trend line equation of plot of each sensor was applied to convert the resistance values of the sensors into concentration of ozone gas in ppm.

Note that the calibation was made in low pressure, which can be applied mainly to starosphere range. It may not be good for atmosphere data. The ozone concentration measured from 0 to 1.00 ppm may have slight different value of slope and y intercept due to some experimental error and leakage.

The trend line equation of the calibration plot is given as:

y (sensor resistance) = [***m*** (slope). ***x*** (concentration of ozone, ppm)] + ***b***(y intercept)

The concentration of ozone gas can be determined by: $x = (y - b)/m$

The trendline equations for each sensors were listed in the following table-1.

Table-1 Trendline Equations determined from the calibration plots shown in fig.7 (a) to (v) of gas sensors

Sensor Box # 1 Concentration of Ozone (=x) (ppm)			
Sensor#		**Sensor#**	
S1-1	**x = (y-996)/13.2**	**S1-5**	**x = (y-1120.8)/13.8**
S1-2	**x = (y-1150.2)/13.6**	**S1-6**	**x = (y-1201)/13.7**
S1-3	**x = (y-1210)/13.75**	**S1-7**	**x = (y-1102)/13.3**
S1-4	**x = (y-1140.2/13.45**	**S1-8**	**x = (y-996.5)/13.1**
Sensor Box#3			
Concentration of Ozone (=x) (ppm)			
Sensor#		**Sensor#**	
S3-1	**x = (y-1550)/20.1**	**S3-5**	**x = (y-1795)/23.7**
S3-2	**x = (y-2100)/23**	**S3-6**	**x = (y-2130)/24.2**
S3-3	**x = (y-2170)/22.6**	**S3-7**	**x = (y-2070)/23.7**
S3-4	**x = (y-1800)/23.7**	**S3-8**	**x = (y-1400)/17.5**

With these equation parameters, we obtained the following the ozone profile plots shown in fig.21 (a) to (p):

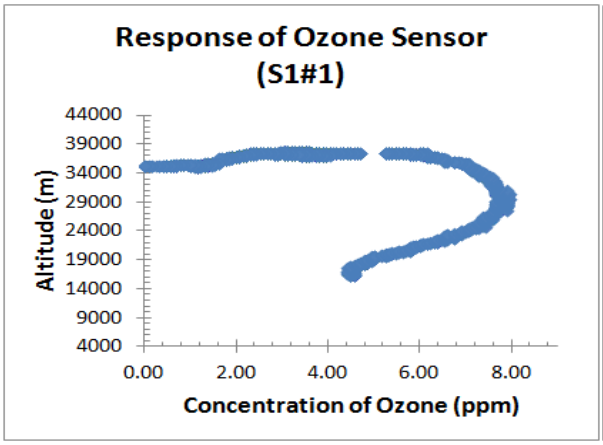

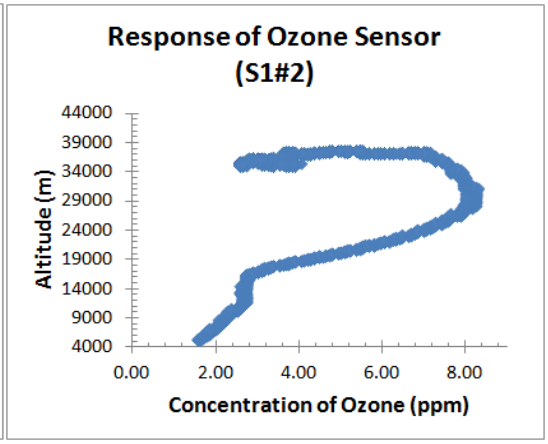

Fig 21(a) Ozone profile of sensor S1#1 Fig 21(b) Ozone profile of sensor S1#2

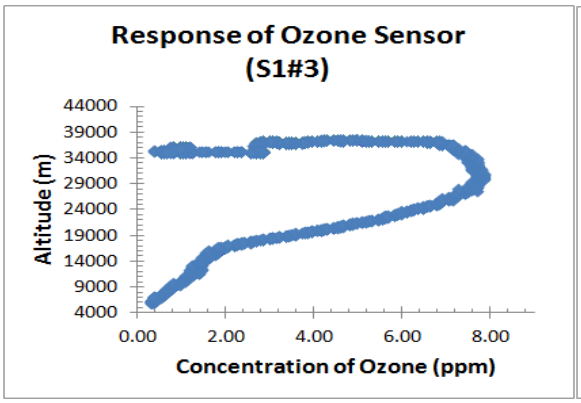

Fig 21(c) Ozone profile of sensor S1#3

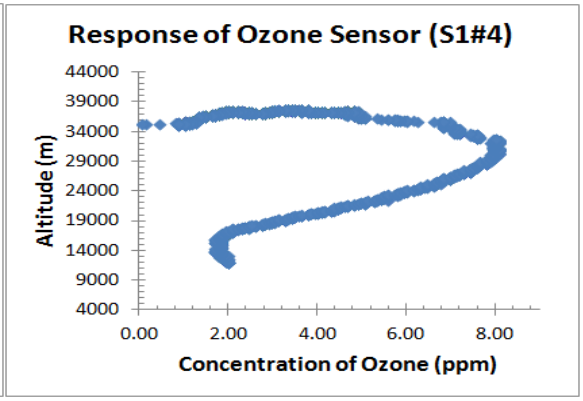

Fig 21(d) Ozone profile of sensor S1#4

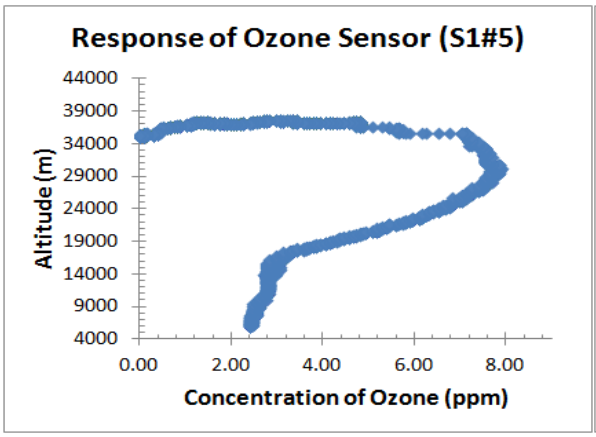

Fig 21(e) Ozone profile of sensor S1#5

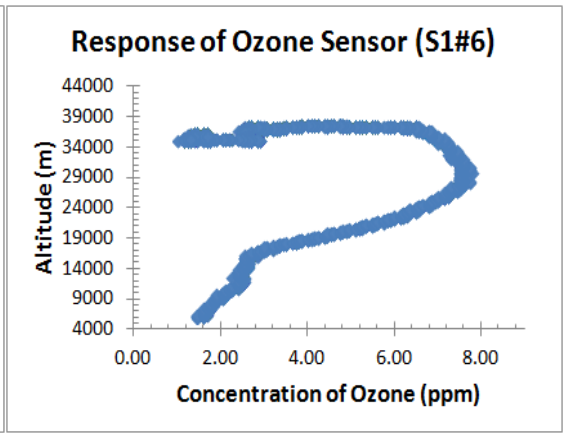

Fig 21(f) Ozone profile of sensor S1#6

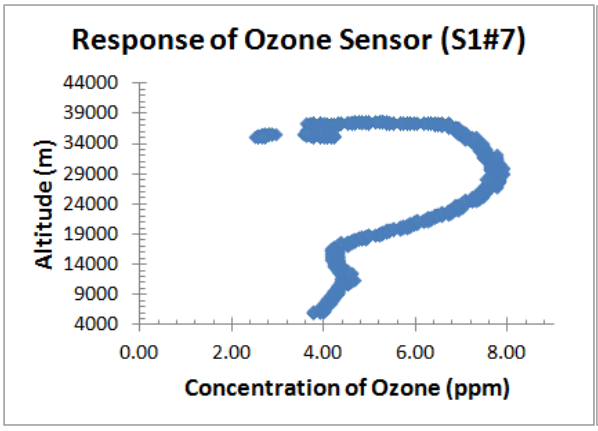

Fig 21(g) Ozone profile of sensor S1#7

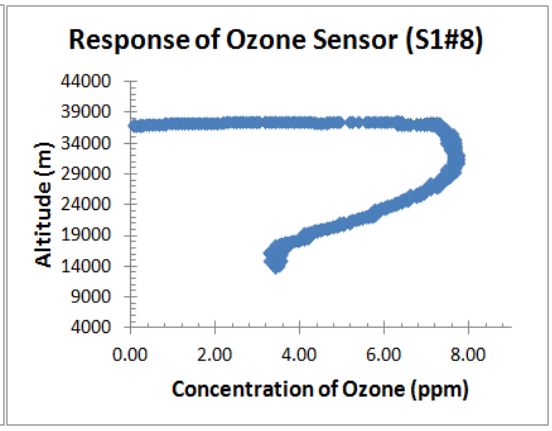

Fig 21(h) Ozone profile of sensor S1#8

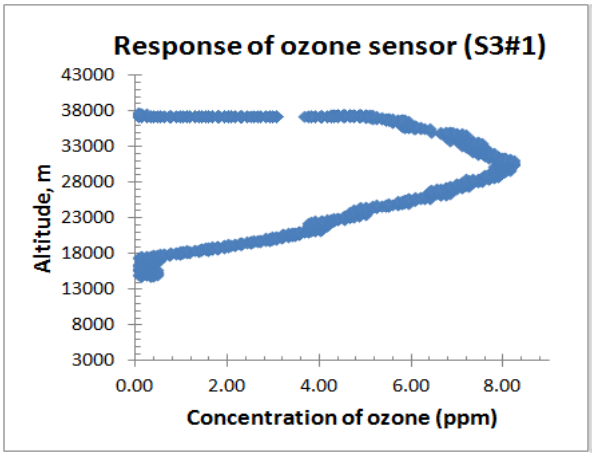

Fig 21(i) Ozone profile of sensor S3#1

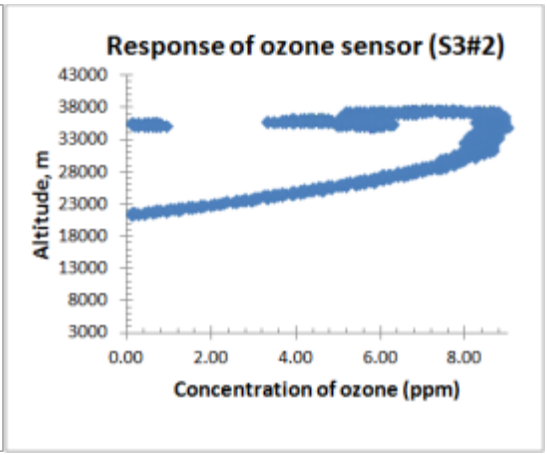

Fig 21(j) Ozone profile of sensor S3#2

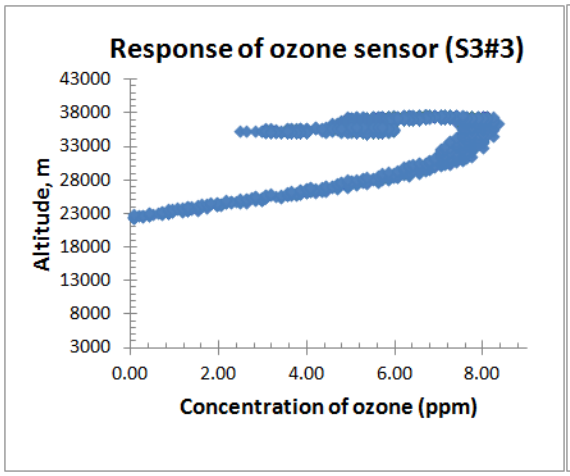

Fig 21(k) Ozone profile of sensor S3#3

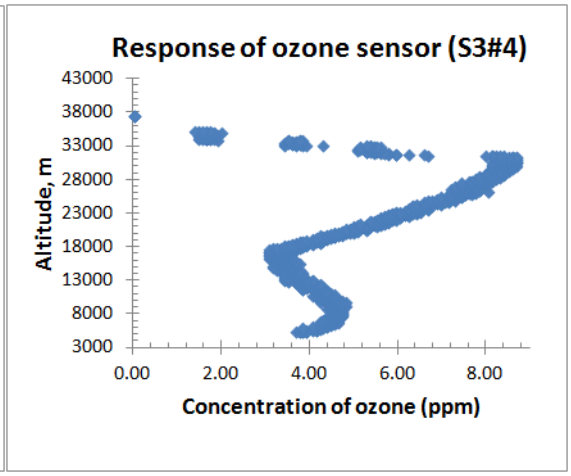

Fig 21(l) Ozone profile of sensor S3#4

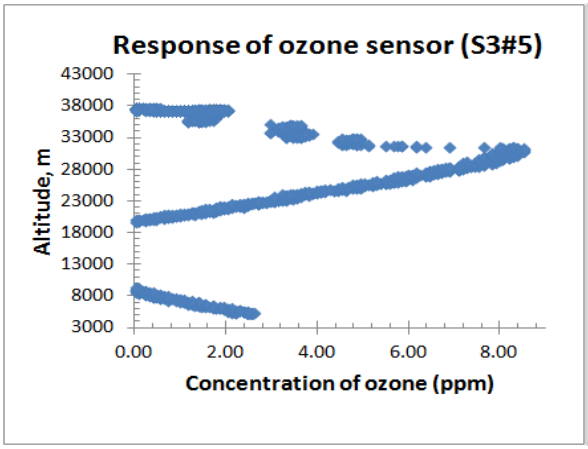

Fig 21(m) Ozone profile of sensor S3#5

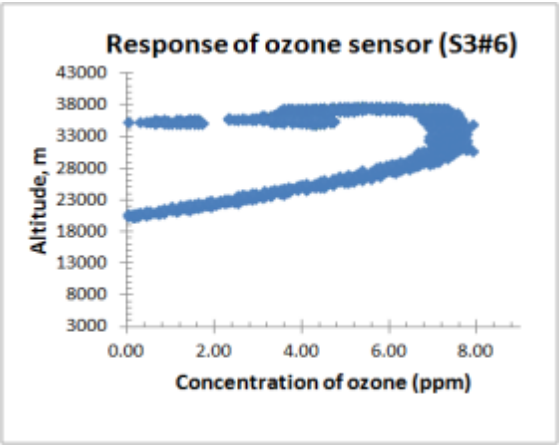

Fig 21(n) Ozone profile of sensor S3#6

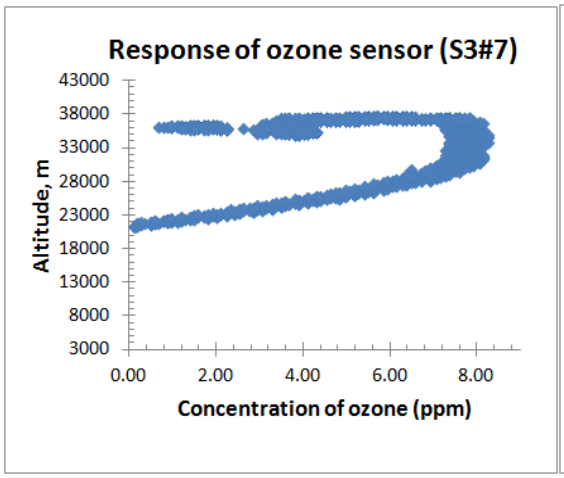

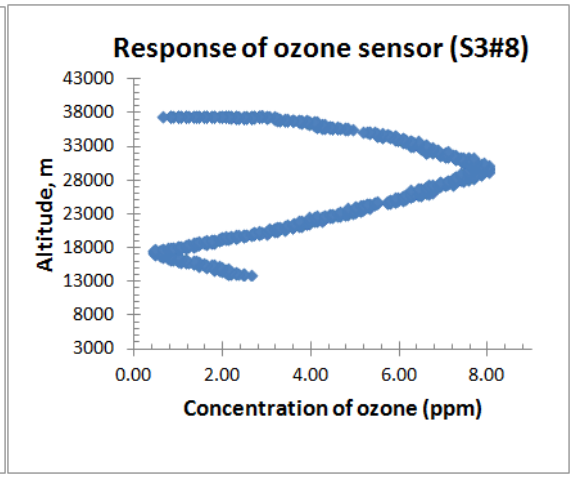

Fig 21(o) Ozone profile of sensor S3#7 Fig 21(p) Ozone profile of sensor S3#8

The nature of ozone profiles measured by three sensors box #1, 3 are nearly matched with the theoretically profile measured and quoted by various research groups, which are shown in Fig. 23 to 26 for the comparison purpose. The measured value of maximum concentration of ozone was observed from 7.5 to 8.0 ppm, which is very close to the expected values. We need to find out some theoretical calculation method to generate theoretical data for comparison.

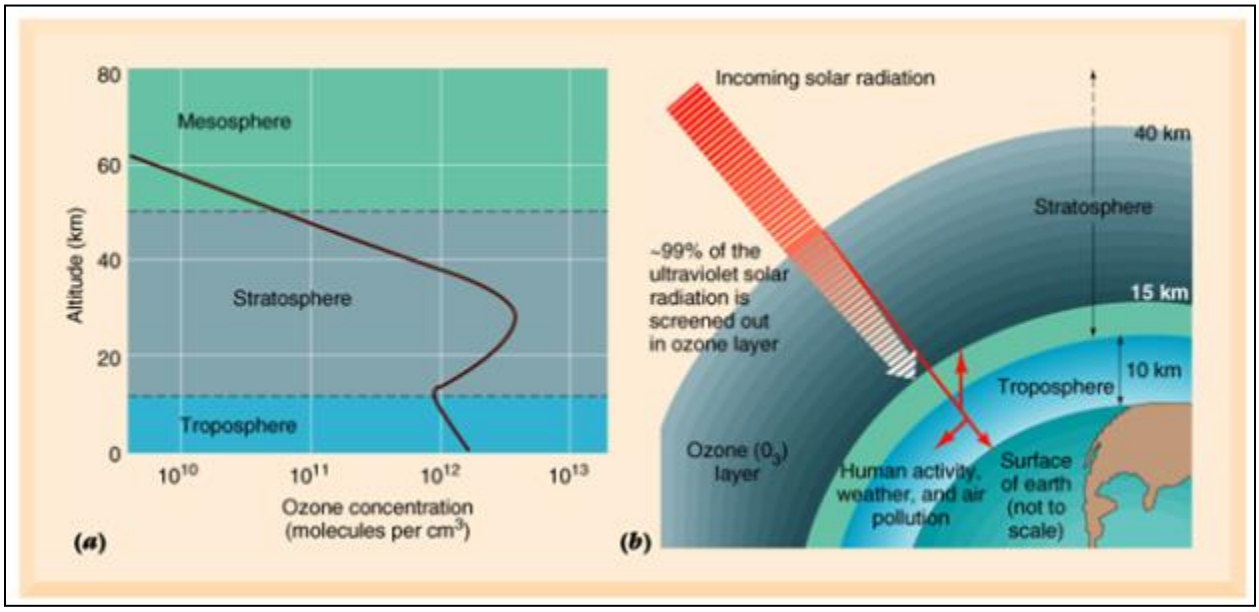

Fig.23 Ozone in the atmosphere

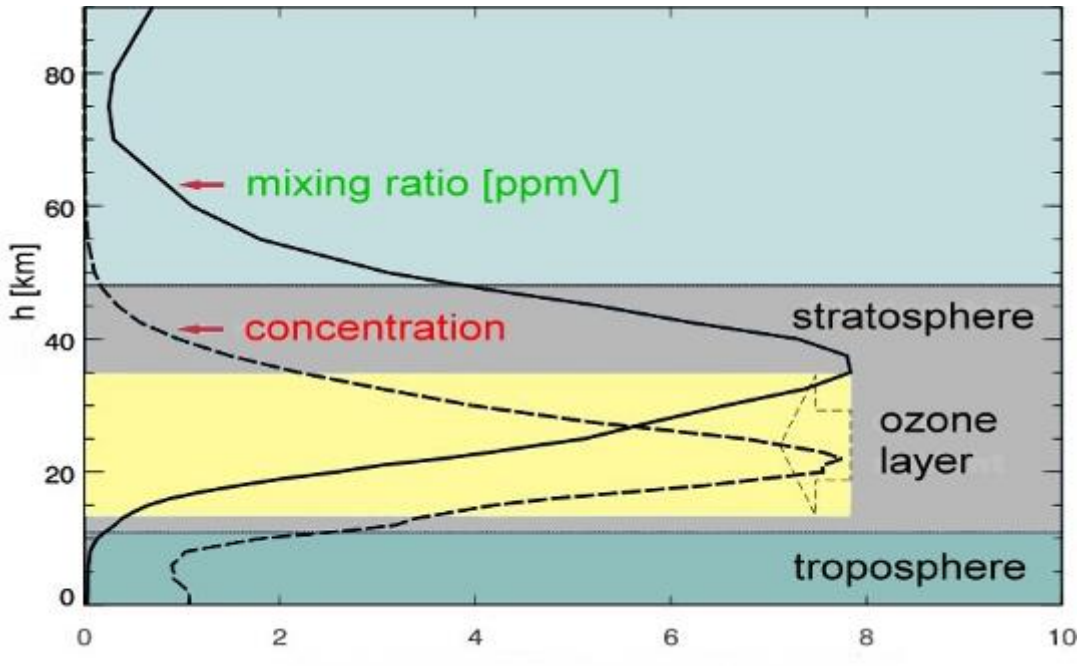

Fig.24 Theoretical ozone profile in stratosphere **(http://www.atmosphere.mpg.de/enid/1yy.html)**

(ppmv = parts per million by volume = volume mixing ratio)

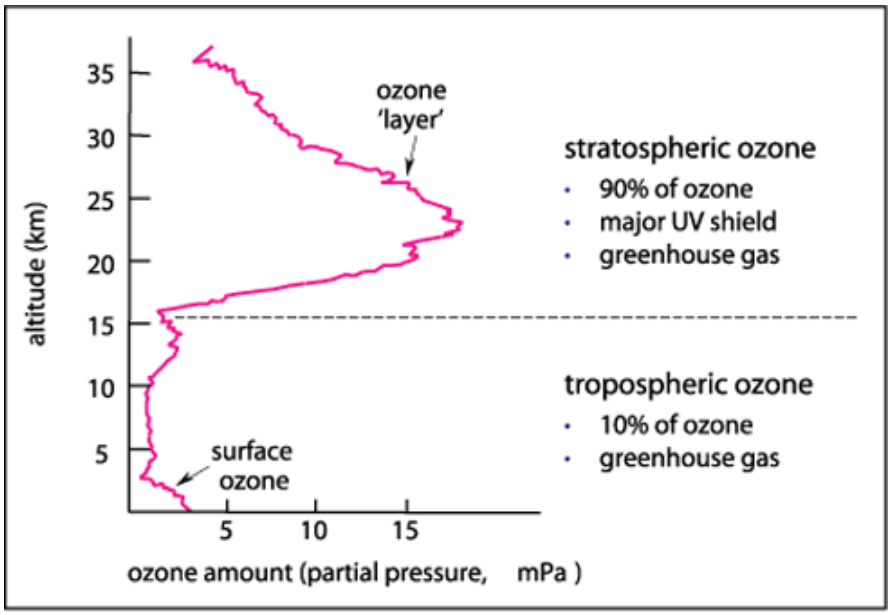

http://www.environment.gov.au/soe/2001/publications/theme-reports/atmosphere/atmosphere03-1.html

Fig.25 Ozone in the atmosphere with its impact

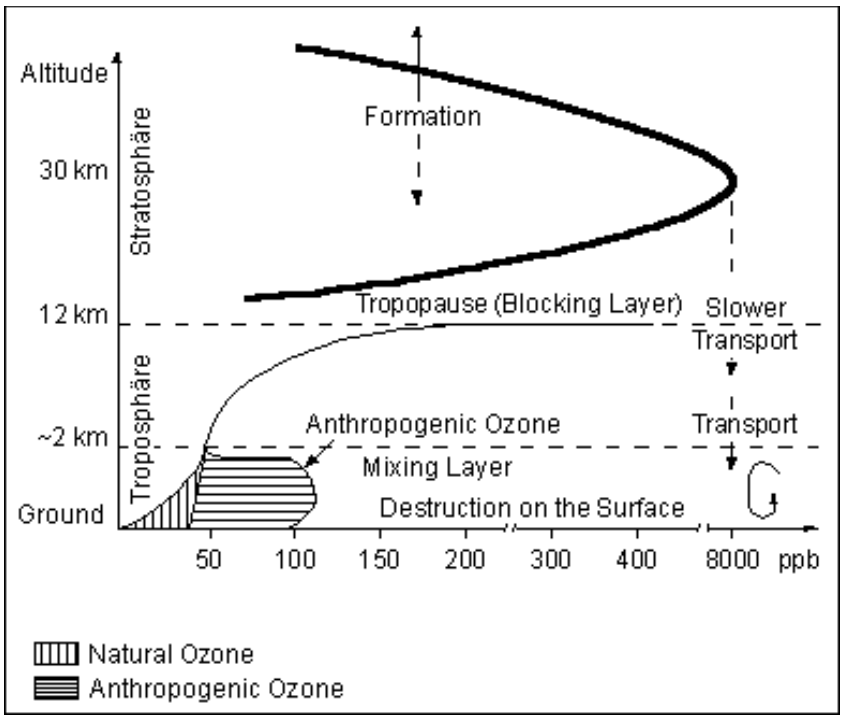

Fig.26 Ozone profile

http://www.stadtentwicklung.berlin.de/umwelt/umweltatlas/ed306_01.htm

Note: Units for measurement of ozone.

In the presence study, we used part per million (ppm) units for determination of ozone concentration. We calibrated our sensors in the closed chamber using a digital ozone meter, which has unit in ppm only.

Ozone is mainly measured by the Dobson spectrometer in Dobson Units (DU). Our sensors are very cheap, smaller in size, low mass and easy to interface with electronic compared to that of Dobson spectrometer.

1 Dobson Unit (DU) is defined to be 0.01 mm thickness of gas at STP (0ºC, 1 atm); the ozone layer represented above is then ~300 DU

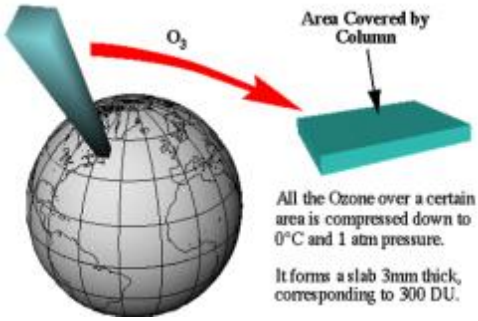

Problems, failure analysis and future plan

(1) Our GPS was failed after 60000 feet. We had updated the new program for GPS this year, but GPS failed again this time. We also had similar problem with the HASP 2011 and 2012 balloon flights. We recovered the altitude data from HASP GPS recorded data after the flight. Our GPS was not certified by Government agency. GPS Units are typically limited to controlled airspace at 60,000 feet and 1000 knots. These are commonly known as the COCOM limits. For anything outside of that, one has to go for a higher-end GPS unit and possibly some additional paperwork with the Government regulation agency. Some of data were lost misalignment of time stamp during switching of GPS from our payload to GPS of HASP.

(2) We also found some of data stream were not in order and were mixed with data of other payload. That issue was with the ground radio station. We filtered out those bugs from the data. Of course, we lost some data during stratosphere.

(3) Pressure sensor was saturated at 110 mbar. We found that that pressure sensor can work only up to 110 mbar. We planned to replace it by high and low range of pressure sensors in the next flight.

(4) Light sensors helped us to verify the science concept of generation of ozone in the presence of UV light. We found from data sheet that the spectral response was not maximum in the UV light but in near visible light. We planned to replace these light sensors by only UV light sensors.

(5) Our nanocrystalline and nanocomposite sensors worked well for detection of ozone gas. We have tested the commercially available ozone sensor (e2V-MiCS-2610) in our lab in the concentration range 2-10 ppm of ozone. But did not worked gave reproducible and linear response. Therefore, we had dropped the idea to add it in our payload for comparison purpose.

(6) We did not able to add a radio circuit in the payload to communicate data in addition to HASP communication link in order to develop ***a free flying payload***. This is because no one was able to visit Fort Sumner, NM for launching of balloon and get the data from radio.

Conclusions:

(i) The improved nanocrystalline ITO thin film gas sensors (Box#1) and nanocomposite ZnO+ITO thin film gas sensors fabricated (Box#3) by the UNF team have good selectivity with ozone gas and worked well during entire flight period and measured the ozone profile of the stratosphere. Even though nanocomposite WO_3+ITO thin film gas sensors (Box#4) have good response with reducing gases, can detect ozone with less

sensitivity. Our science objectives of all these sensors were successfully tested and scientifically verified. We will modify the composition of WO_3+ITO and make it more selectivity for the reducing gas and will use it to measure reducing gases in atmosphere and troposphere during next HASP2014 flight.

(ii) Light sensor proved the presences of UV light, which are responsible to generate more ozone gas by converting oxygen into ozone.

(iii) Improved temperature control circuit and software program gave better stability of temperature of sensors during entire flight period.

(iv) Improved version of microcontroller circuit and software handle all sensors data and faster conversion of RAW file into EXCEL file.

(v) After recovery of payload, we tested the payload, circuit and all sensors and found all parts in good working condition.

(vi) UND-UNF team is interested to make further improve sensors payload and seeking another opportunity for the HASP 2014 flight.

Acknowledgements

We are very grateful to

(i) Dr. Gregory Guzik and Mike Stewart, HASP-LSU for their continue help, cooperation and encouragement. We also appreciate help of Doug Granger for his support.

(ii) Columbia Scientific Balloon Facilities (CSBF)-NASA, Palestine TX and Fort Sumner, NM, and team of CSBF.

(iii) Florida Space Grant Consortium for providing the financial support to UNF team.

(iv) Dr Jaydeep Mukherjee, Director, Florida Space Grant Consortium (FSGC) and Ms. Sreela Mallick, FSGC for their valuable help and encouragement.

(v) North Dakota Space Grant Consortium for providing the financial support to UND team.

(vi) Websites links mentioned in this report for using their pictures to explain the science of this report. We intention is not to violate any copyright, but only education and research purposes.